iScience

CellPress
OPEN ACCESS

Article

High-throughput screening for myelination promoting compounds using human stem cell-derived oligodendrocyte progenitor cells

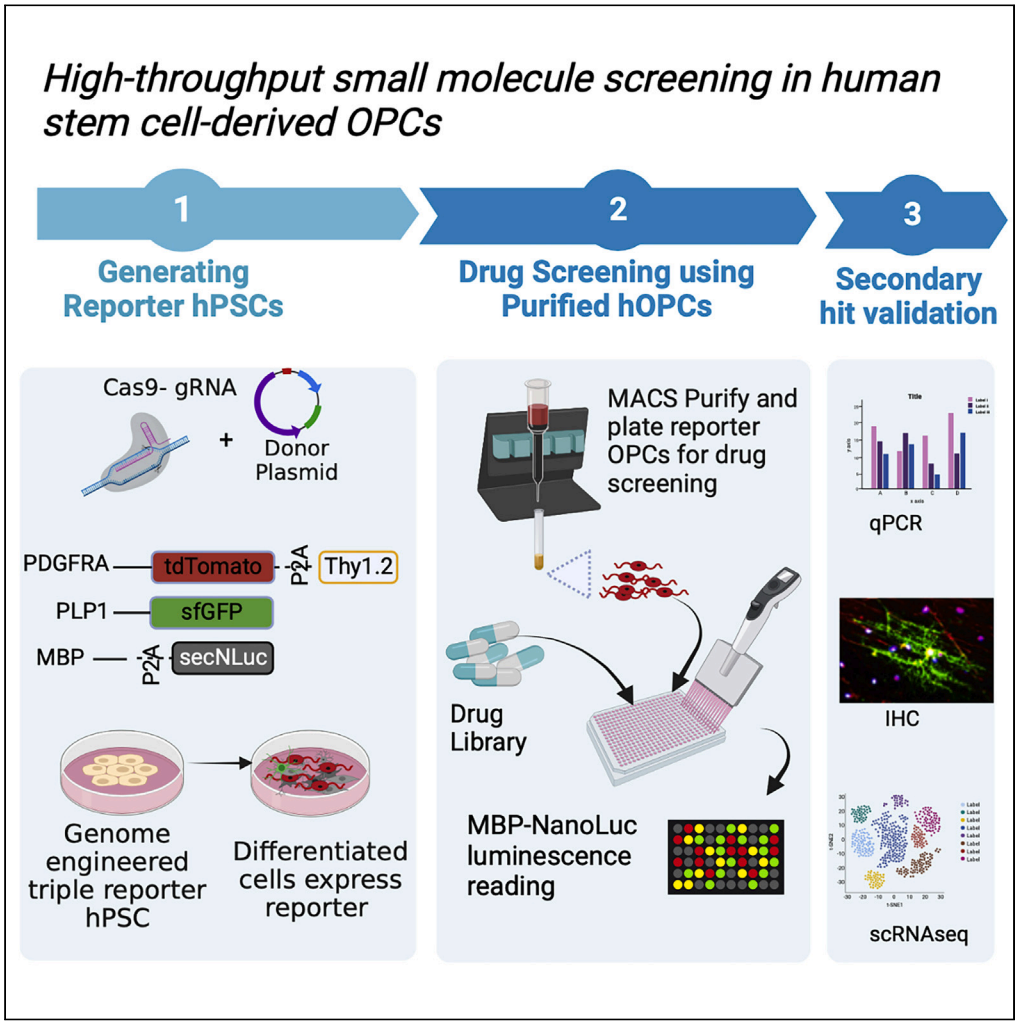

Weifeng Li, Cynthia Berlinicke, Yinyin Huang, ..., Stephen Madden, Donald J. Zack, Xitiz Chamling

xchamli1@jhmi.edu

Highlights

CRISPR-engineered triple reporter hPSC line to study oligodendrocyte lineage cells

A high-throughput drug screening using human oligodendrocyte precursor cells

HTS with hOPCs identified Ro1138452 and SR2211, two myelination promoting molecules

scRNAseq on hOPCs treated with the two molecules highlights modulated pathways

Li et al., iScience 26, 106156
March 17, 2023
https://doi.org/10.1016/j.isci.2023.106156

iScience

CellPress
OPEN ACCESS

Article

High-throughput screening for myelination promoting compounds using human stem cell-derived oligodendrocyte progenitor cells

Weifeng Li,[1] Cynthia Berlinicke,[2] Yinyin Huang,[3] Stefanie Giera,[4] Anna G. McGrath,[4] Weixiang Fang,[5] Chaoran Chen,[5] Felipe Takaesu,[6] Xiaoli Chang,[2] Yukan Duan,[2] Dinesh Kumar,[3] Calvin Chang,[7] Hai-Quan Mao,[7,8] Guoqing Sheng,[4] James C. Dodge,[4] Hongkai Ji,[5] Stephen Madden,[3] Donald J. Zack,[1,2,9,10] and Xitiz Chamling[2,11,12,*]

SUMMARY

Promoting myelination capacity of endogenous oligodendrocyte precursor cells (OPCs) is a promising therapeutic approach for CNS demyelinating disorders such as Multiple Sclerosis (MS). To aid in the discovery of myelination-promoting compounds, we generated a genome-engineered human pluripotent stem cell (hPSC) line that consists of three reporters: identification-and-purification tag, GFP, and secreted-NanoLuc, driven by the endogenous *PDGFRA, PLP1,* and *MBP* genes, respectively. Using this cell line, we established a high-throughput drug screening platform and performed a small-molecule screen, which identified at least two myelination-promoting small-molecule (Ro1138452 and SR2211) that target prostacyclin (IP) receptor and retinoic acid receptor-related orphan receptor γ (RORγ), respectively. Single-cell-transcriptomic analysis of differentiating OPCs treated with these molecules further confirmed that they promote oligodendrocyte differentiation and revealed several pathways that are potentially modulated by them. The molecules and their target pathways provide promising targets for the possible development of remyelination-based therapy for MS and other demyelinating disorders.

INTRODUCTION

Multiple sclerosis (MS) is an immune-mediated demyelinating disease in which the immune system attacks and degrades myelin sheaths of neuronal axons in the central nervous system (CNS).[1] Damage and loss of a neuron's myelin sheath can cause apoptosis of the myelin producing oligodendrocyte cells, axonal damage and neuronal cell death, which ultimately can lead to neurological disabilities.[2] All currently approved therapies for MS act by modulating the patient's immune response. Such therapies can help to slow down the progression of the disease, but do not directly promote the remyelination that is needed to improve the long-term function and survival of damaged neurons. A number of studies have shown that following myelin damage, oligodendrocyte progenitor cells (OPCs) and neural precursor cells (NPCs) migrate toward the site of injury, where they demonstrate some ability to differentiate into mature oligodendrocytes that are capable of remyelinating the demyelinated axons.[3,4] However, endogenous progenitors around a CNS lesion appear to be limited in both their mitotic competence and differentiation potential, and they progressively lose their remyelination capacity with aging.[5,6] If we could employ biologically active molecules to stimulate the ability of endogenous OPCs to differentiate and produce new myelin, this could have great therapeutic value for MS and other demyelinating diseases.

Drug screening to identify molecules that promote OL maturation and myelination has been performed using primary rodent OPCs[7,8] and mouse ES-derived OPCs.[9] The advent of human pluripotent stem cells (hPSC)-derived OPCs and OLs now make it possible to perform such drug screening using human cells, which presumably would be more clinically relevant to human disease. However, to our knowledge, no platforms that utilize human OPCs to screen for myelin promoting compounds have yet been reported. Use of hPSC-derived, physiologically relevant cells for drug screening to identify molecules that promote remyelination is limited by the difficulty in obtaining large quantities of pure, disease relevant cell-types such as

[1]Department of Genetic Medicine, Johns Hopkins University School of Medicine, Baltimore, MD 21287, USA

[2]Department of Ophthalmology, Wilmer Eye Institute, Johns Hopkins University School of Medicine, Baltimore, MD 21287, USA

[3]Sanofi Inc., Translational Science, 350 Water Street, Cambridge, MA, 02141, USA

[4]Sanofi Inc., Rare and Neurologic Diseases Therapeutic Area, 350 Water Street, Cambridge, MA, 02141, USA

[5]Department of Biostatistics, Johns Hopkins Bloomberg School of Public Health, Baltimore, MD 21205, USA

[6]Wallace H. Coulter Department of Biomedical Engineering, Emory University School of Medicine & Georgia Institute of Technology, Atlanta, GA, USA

[7]Department of Biomedical Engineering, Johns Hopkins School of Medicine, Baltimore, MD 21205, USA

[8]Institute for NanoBioTechnology, Johns Hopkins University, Whiting School of Engineering Baltimore, MD 21218, USA

[9]The Solomon H. Snyder Department of Neuroscience, Johns Hopkins University School of Medicine, Baltimore, MD 21205, USA

[10]Department of Molecular Biology and Genetics, Johns Hopkins University School of Medicine, Baltimore, MD 21287, USA

Continued

OPCs.[10] In addition, the majority of the OL maturation assays either use immunofluorescence analysis to measure the amount of MBP, or use image-based morphological analysis to detect cells that resemble oligodendrocytes.[7–9,11,12] Although such image-based, high-content screening (HCS) assays can be powerful, morphology-based assays have limited sensitivity and they are also less scalable. Here, we used CRISPR/Cas9-based genome editing to generate a triple reporter hESC line where an identification-and-purification (IAP) tag,[13] GFP, and secreted Nanoluciferase (secNluc) reporters were engineered to be driven by the endogenous *PDGFRA, PLP1* and *MBP* genes, respectively. Once the reporter hESC is differentiated, the PDGFRA expressing OPCs can be immuno-purified using the IAP tag,[13,14] and the time and efficiency of oligodendrocyte maturation can be quantified via the expression of GFP and secNluc. These qualities enabled us to use the reporter cell line to develop a highly sensitive and scalable screening platform for discovery of myelination promoting compounds that: 1) uses purified human OPCs, 2) allows time-course assays to follow real-time expression of oligodendrocyte/myelination markers, and 3) makes it possible to perform Nluc-based HTS and image-based HCS using the same cell cultures.

The hOPCs derived from this reporter system was used to screen 2500 bioactive molecules, resulting in the identification of several molecules that function at nanomolar doses to enhance maturation of oligodendrocytes from OPCs. In addition to a number of already known myelination promoting molecules, at least two compounds that have not been previously reported to improve OL differentiation and enhance myelination were identified by this screen. Image-based analysis and electrospun nanofiber-based *in vitro* myelination assays further validated the effect of these compounds on hOPCs-hOL maturation. In addition, we validated the efficacy of these compounds in a different hPSC-OPC reporter cell line. Furthermore, we performed scRNAseq to examine the biological processes in OPCs and OLs that are modulated by treatment with these small molecules. The identified compounds and their target pathways provide promising new potential targets for the development of remyelination-based therapies for the demyelinating diseases.

RESULTS

Generation of a hESC triple-reporter system

We previously engineered a hESC reporter cell line (PDTT) that allows identification and purification of hESC-derived, PDGFRA expressing oligodendrocyte lineage cells (OLLCs).[13] Here, we added two more reporter sequences to the PDTT line, generating a reporter system that is suitable for high throughput screening (HTS) as well as HCS. CRISPR-Cas9-based genome editing was used to knock-in super-fold GFP (sfGFP) and secNluc reporter sequences before the stop codons of the *PLP1* and *MBP* genes, respectively (Figure 1A). The PLP1-sfGFP construct generates a fusion reporter whereas the MBP-P2A-secNluc construct leads to two separate proteins (MBP and secNLuc) due to the presence of a self-cleaving P2A peptide.[15]

Before knocking in the P2A-secNluc reporter into the *MBP* locus, we wanted to confirm that the secNLuc protein product, following its P2A-mediated separation, is successfully secreted into the extracellular culture media and retains enzymatic activity. Therefore, we transfected a CMV-tdTomato-P2A-secNluc plasmid into HEK293 cells and confirmed that the culture media of the transfected cells has Nluc activity (Figures S1A–S1C).

The final reporter system that we generated (PTt-P1-MsNL) incorporates three reporters: 1) PDGFRA-P2A-tdTomato-P2A-Thy1.2 (or an IAP tag), in which, on *PDGFRA* expression, tdTomato as well as Thy1.2 are produced. tdTomato localizes to the cytoplasm whereas Thy1.2 localizes to the cell surface, allowing the PDGFRA expressing cells to be immunopurified via Thy1.2 antibody conjugated magnetic microbeads[13]; 2) PLP1-sfGFP, where expression of sfGFP is driven by *PLP1*; and 3) MBP-P2A-secNLuc, where NLuc protein is secreted into the cell culture media, allowing serial sampling and serial quantitative readout of *MBP* expression (Figures 1A and S1D–S1F).

Validation of the reporter cell line

With the PTt-P1-MsNL reporter line, similar to the PDTT cell line, PDGFRA-tdTom+ cells appear around day 45 of differentiation in our culture system.[13] PLP1-GFP+ cells are visible as early as day 60. As the culture matures, less tdTomato+ cells and more GFP expressing cells are detected, and more MBP/sNLuc is also produced (Figures 1C and S2). The GFP+ cells have processes and morphology that resemble oligodendrocyte cells (Figure 1D). Moreover, the majority of GFP+ cells also express low levels of tdTomato,

[11]Department of Neurology, Johns Hopkins University School of Medicine, Baltimore, MD 21287, USA

[12]Lead contact

*Correspondence: xchamli1@jhmi.edu

https://doi.org/10.1016/j.isci.2023.106156

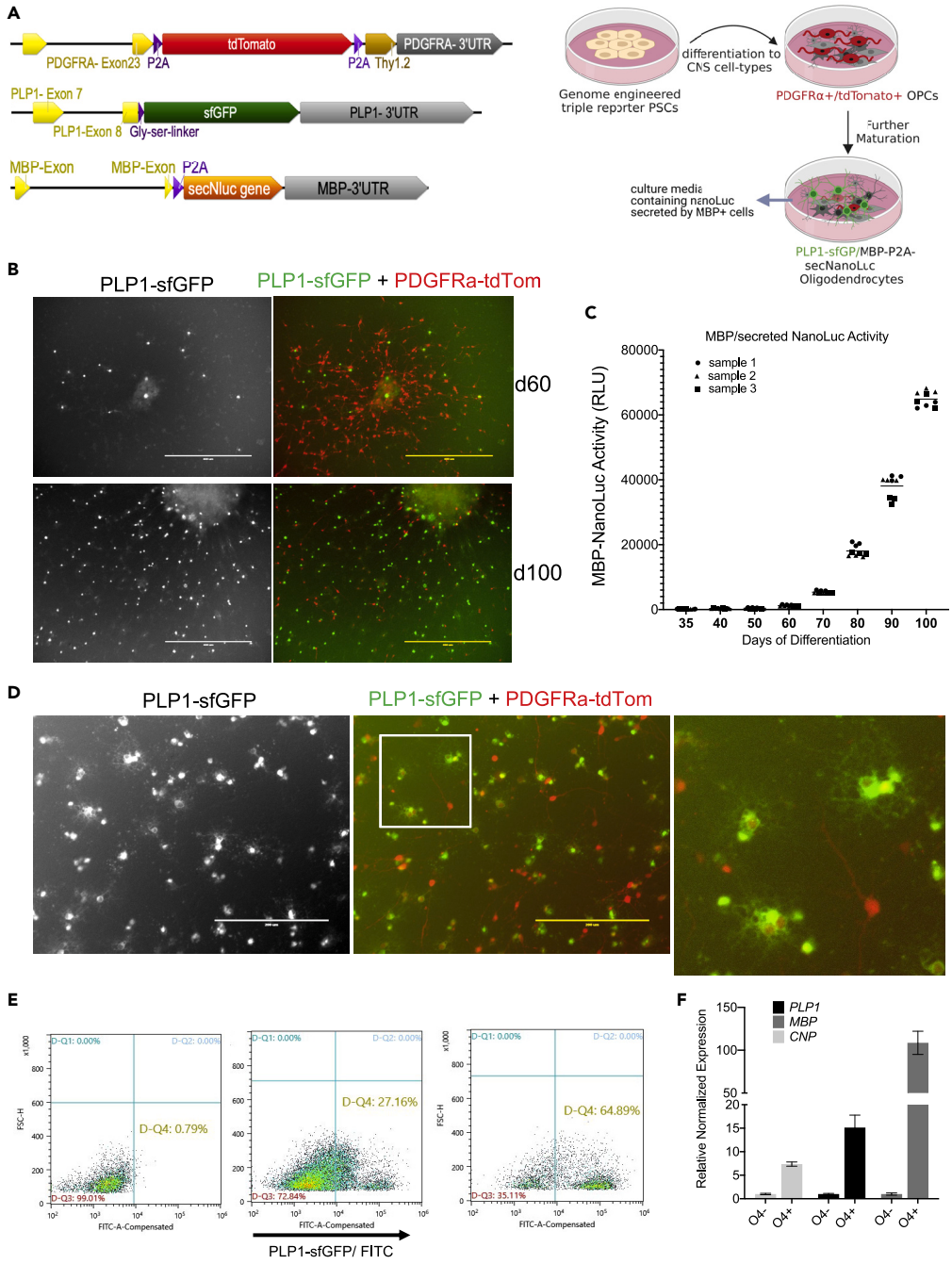

Figure 1. Generation and validation of an advanced hES reporter system

(A) Schematic of the endogenous *PDGFRA*, *PLP1* and *MBP* locus of the Ptt-P1-MsnL reporter line after CRISPR-Cas9-based genetic knock-in of reporter sequences.

(B) Expression of the tdTomato and sfGFP fluorescent reporters in the differentiating oligodendrocyte cultures Scale bar: 400 μm

(C) secNluc activity in the cell culture medium of differentiating PtT-P1-MsNL reporter line measured with Nano-Glo assay. Culture media from different days of differentiation (xaxis) were removed for the assay. Increase in Nano-Luc activity (yaxis), which corresponds to MBP expression increases as cells mature.

(D) A higher magnification image of the reporter expression on d100 culture shown in (B). GFP+ processes and branches resembling oligodendrocytes morphology are further magnified in the inset. Scale bar: 200 μm

(E) MACS-based enrichment of the GFP+ cells using O4 antigen microbeads. 60% GFP+ cells were achieved from d105 cells.

(F) qPCR shows enrichment of OL markers in the O4+ cells compared to the O4- cells. Data presented as mean +/- SEM

which indicates that these cells originated from PDGFRa expressing progenitor cells (Figures 1D and S2). We also demonstrate that an antibody against O4, an antigen specific to pre-oligodendrocyte cells, can be used to enrich PLP1-GFP+ cells from the differentiating OLLC culture (Figures 1E, 1F, and S3C). Essentially, in this advanced reporter cell-line, PDGFRA+ OLLCs can be temporally purified,[13] mature OLs can be identified and enriched for using the expression of PLP1-sfGFP, and the NLuc activity, which represents MBP expression, can be quantitated over time using a small aliquot of cell culture media.

Optimization of the high throughput screening platform

An advantage of our reporter system is that it does not require fixation or lysis for assessment, which allows us to perform time-course assays to follow real-time expression of *PLP1* and *MBP*, oligodendrocyte/myelination marker genes. Because our main goal in generating the described reporter system was to perform HTS, we went on to optimize our assay for use in a 384-well plate format. The seeding density, NanoGlo reagent volume, culture media volumes, and the time course of the assay were optimized in preliminary studies (Figures S4A and S4B) (see the STAR Methods section). Although T3 is commonly used as positive control for OPC to OL maturation in rodent cells, we found that T3 has only a very mild effect on human OPCs (Figure 2D). Therefore, we decided to use Tasin-1 instead of T3 as a positive control and DMSO was used as negative control for optimization of our assay (Figures 2A and S4C–S4F). Tasin-1 is an inhibitor of Emopamil binding protein (EBP) and a known inducer of OL differentiation and myelination.[11]

To establish our screening assay (Figure S5), PDGFRA-tdTomato+ OPCs from d75-d85 differentiation cultures were purified by magnetic-activated cell sorting (MACS) with Thy1.2 microbeads and then plated into 384-well plates. We noticed a small degree of well-to-well variation in the day 0 Nluc activity (relative light unit (RLU) values), which was likely caused by small differences in the number of cells plated per well (Figure S4C). To control for this variability, instead of using absolute RLUs to compare effects of compounds on the cells, we used fold change (FC), which was calculated for each well by dividing a "time-point" RLU of a well by day 0 RLU of the same well (Figures 2A–2C). The FC value had better z' factor values (−0.27 in FC vs −0.37 in raw RLU at d10 time-points) and better relative standard deviation (16% in FC vs 29% in raw RLU at d10 time-point) while retaining the significance of the results (Figures 2A and 2B). Therefore, RLU fold change values calculated at day 5, 10 and 15 (Figure 2C) were used as readouts for our assay.

The screening assay was validated using a number of previously reported OPC differentiation promoting compounds, and the majority of them showed a dose dependent effect on MBP-secNluc expression (Figure 2D). We have also established an *in vitro* myelination system where purified hOPCs are plated on electrospun nanofibers. The plated OPCs align their processed to the nanofibers as early as two days after plating, and within three weeks they mature into OLs and often myelinate the fibers as observed by PLP1-GFP+ processes (Figure S6) or by immunostaining for MBP protein.[13] An increased number of PLP1-GFP+ processes aligning and potentially myelinating the nanofibers, within 10 days in culture, was observed only in the presence of a few compounds, such as Tasin-1 and Quetiapine (Figure 2E).

High throughput screen identifies compounds that increase OL maturation

Using the above-described PT-P1-MsNL-based assay system, we screened the Library of Pharmacologically Active Compounds (LOPAC) and TOCRIS small molecule libraries (Tocriscreen Plus) (~2500 compounds total). For an initial screen, two doses (250 nM and 1.25 μM) of the LOPAC compounds and three doses (100 nM, 500 nM, 2.5 μM) of the TOCRIS compounds were tested (Figures 3A and 3B, Table S1). A total of 240 compounds (120 from each library) that showed FC increases in secNLuc activity that were greater than two standard deviations above the DMSO vehicle control wells were retested at 7 doses (15 nM–11 μM) in duplicate, each at three time-points (5, 10 and 15 days) (Figure 3C, Table S1).

The majority of the hit compounds identified in our screen have known targets, including dopaminergic, adrenergic, and cholinergic receptor signaling, cox, DNA repair, GABA uptake, opioid, P450/cholesterol biosynthesis, and selective estrogen receptor modulators (SERMs) (Figure 3C, Table 1) that have been identified from previous screens using rodent OPCs.[16–18] We also identified a number of targets and molecules that have been implicated but not well studied in OL biology such as Butyryl cholinesterase[19–21] (Tetraisopropyl pyrophosphoramide), BET bromodomain inhibitors[22,23] (I-BET151 and SGC-CBP30), and an NMDA receptor blocker (Ro 25–6981 maleate).[24–27] Most interestingly, we also identified two potent compounds that have not been previously reported to promote OL maturation or myelination, namely

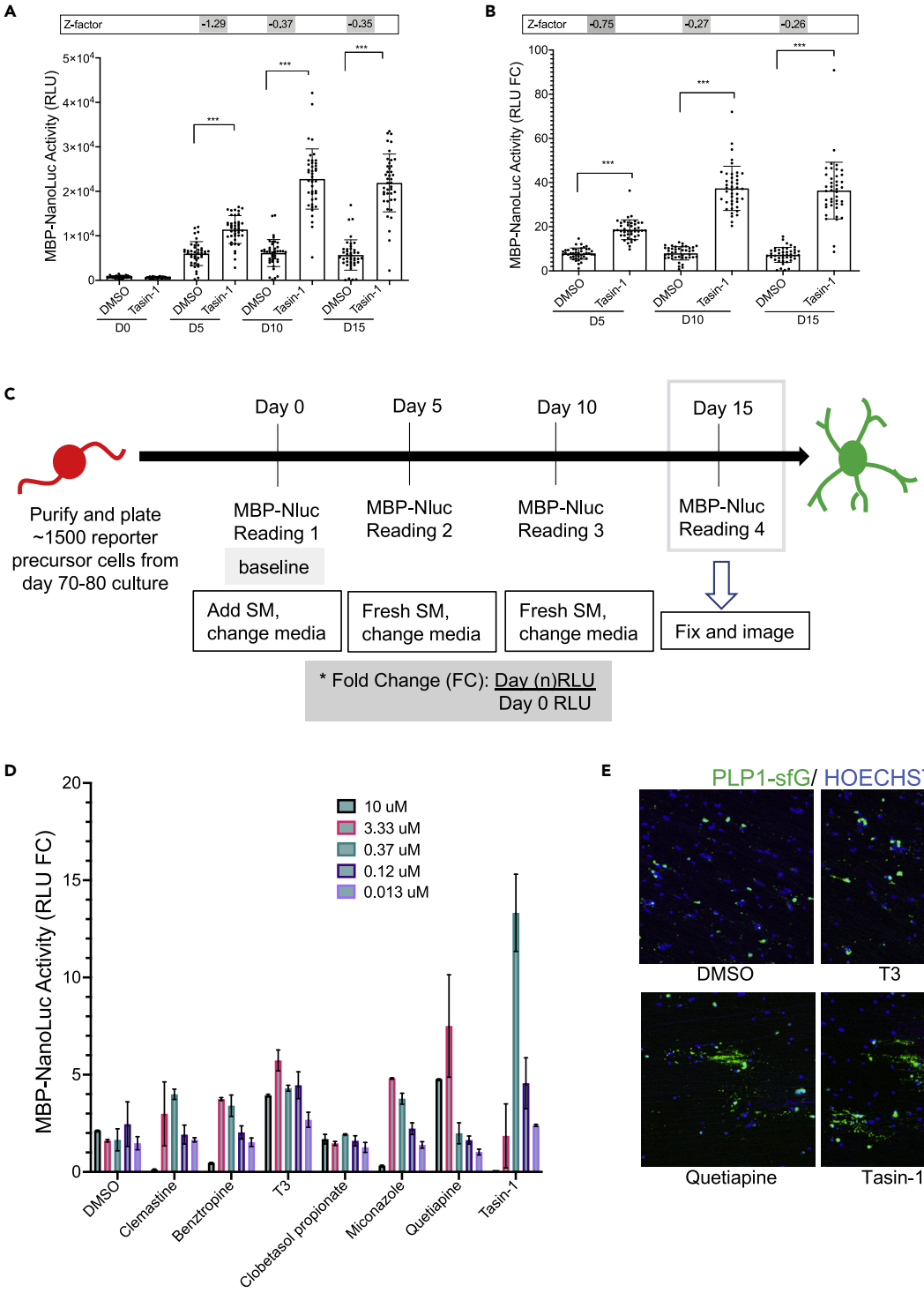

Figure 2. Drug screening assay optimization and validation

(A and B) Effect of 250 nM Tasin-1 in MBP-NLuc expression at days 5, 10, and 15 presented as (A) raw RLU value and (B) RLU fold change (FC). The Z-factor score for FC is better than the raw RLU value. Data presented as mean and compared to DMSO using one-way ANOVA (***, P <0.0001).

(C) Timeline of the drug screening assay used for our reporter cell system.

(D) Validation of our drug screening assay using the compounds known to enhance oligodendrocyte differentiation. Data presented as mean ±SEM.

(E) purified OPCs were plated on a plate containing electrospun nanofiber in the presence of DMSO or small molecules from (D). At least two of the compounds seems to increase the myelination of the nanofiber.

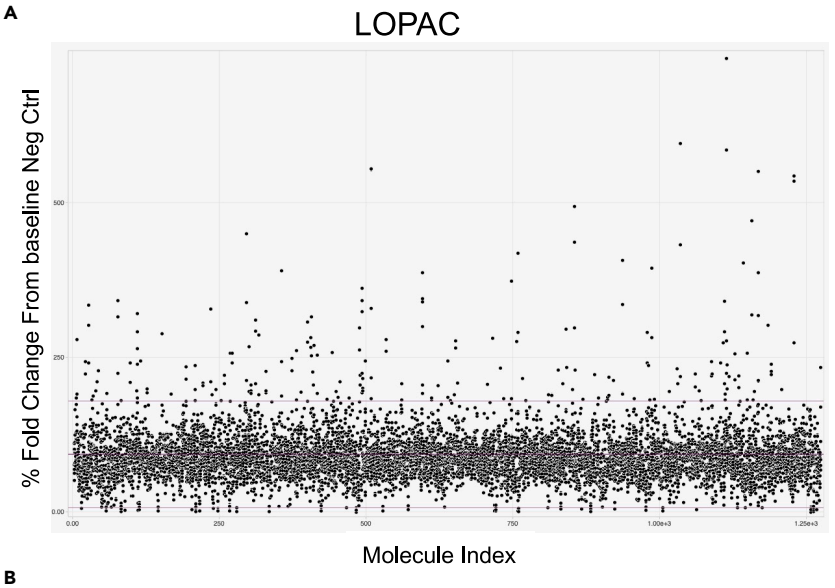
A
LOPAC
% Fold Change From baseline Neg Ctrl
Molecule Index

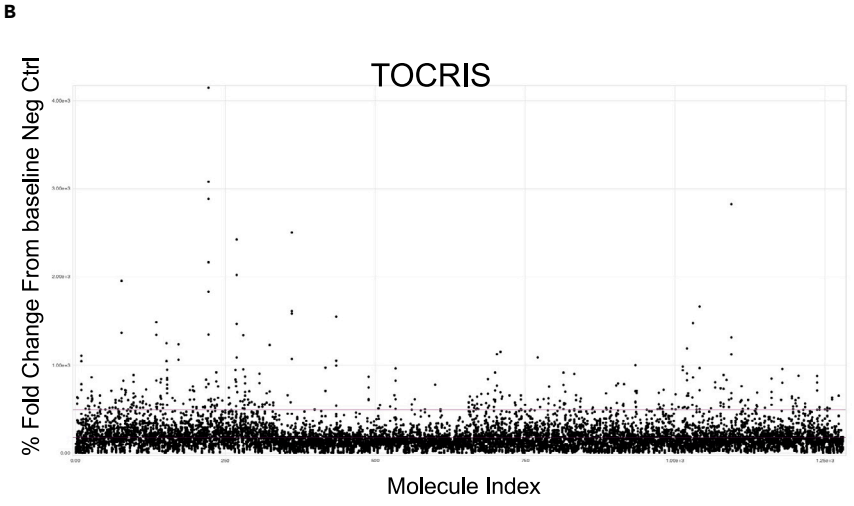
B
TOCRIS
% Fold Change From baseline Neg Ctrl
Molecule Index

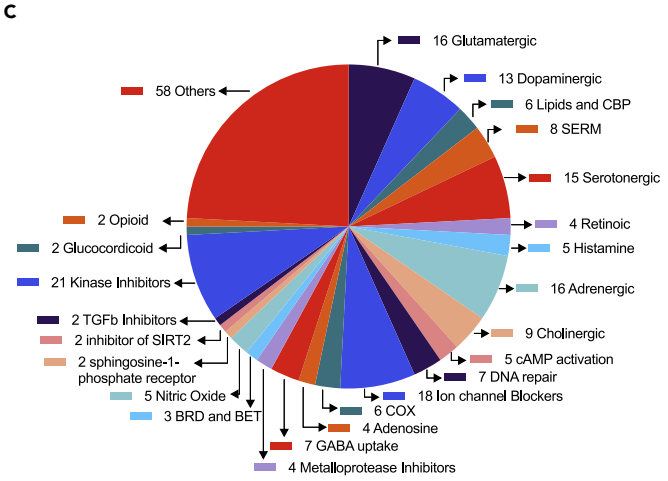
C
16 Glutamatergic
13 Dopaminergic
6 Lipids and CBP
8 SERM
15 Serotonergic
4 Retinoic
5 Histamine
16 Adrenergic
9 Cholinergic
5 cAMP activation
7 DNA repair
18 Ion channel Blockers
6 COX
4 Adenosine
7 GABA uptake
4 Metalloprotease Inhibitors
3 BRD and BET
5 Nitric Oxide
2 sphingosine-1-phosphate receptor
2 inhibitor of SIRT2
2 TGFb Inhibitors
21 Kinase Inhibitors
2 Glucocordicoid
2 Opioid
58 Others

Figure 3. High throughput screening for compounds that enhance oligodendrocyte differentiation

(A and B) Scatterplot of the HTS for compounds that increase activity of MBP-driven secNLuc in the culture media. Plot represents fold change of secNLuc activity versus the compound ID for (A) LOPAC and (B) TOCRIS library of small molecules.

(C) A total of 240 compounds with some effect to increase MBP-NanoLuc expression are graphed as a pie-chart according to a class they fall on. The numbers indicate the number of molecules that fall on that class.

Ro1138452 and SR2211 that target the IP (prostacyclin) receptor pathway and retinoic acid receptor-related orphan receptor γ (RORγ), respectively.

Validation of the promising hit compounds

To validate the Nluc-based screening result (Figure 4B) that our potential hit compounds indeed enhance OPC maturation into OLs in the human cell system, we performed immunohistochemistry (IHC), flow and qPCR analysis of hOPCs treated with Ro1138452 and SR2211, the two most promising small molecules identified from our screen. Flow analysis showed a slight increase in percentage of PLP1-GFP positive cells (Figures 4C and S7), but no change in the PDGFRA-tdTom+ cells was detected. qPCR on OL and OPC marker genes showed increased expression of mature OL associated genes such as *MBP, PLP1* and *MOBP* (Figure 4D). IHC using an antibody against MBP showed a higher number of MBP+ cells in the hOPCs treated with Ro1138452 and SR2211 (Figures 4A and S6C). Furthermore, in our *in vitro* myelination assay, hOPCs treated with these molecules for 10 days align their processes to the nanofibers and appear to myelinate them better than DMSO treated cells (Figure 4A, lower panel). Because Ro25-6981 maleate was detected as a potential hit in both LOPAC and TOCRIS library (Table 1), we examined its effect in the *in vitro* myelination assay. Similar to the Ro1138452 and SR2211 treatment, the Ro25-6981 treatment also appear to promote myelination of the nanofiber.

To further validate the compounds that we identified using our triple reporter system, we generated another dual reporter system (PDGFRA-P2A-tdTomato-P2A-Thy1.2 and MBP-P2A-secNluc) in an independent, male hESC line (RUES1)[28] and named it RPD-MsNL (Figure 5). MACS-purified PDGFRA-tdTomato expressing OPCs generated from the RPD-MsNL hESC reporter line express other OLC markers and also produce secNluc as expected (Figures 5A, 5B, and S8). Next, we cultured the RPD-MsNL-derived OPCs in the presence of Ro1138452 and SR2211 and validated the activity of these compounds in this independent cell line via the Nluc activity, qPCR, IHC and nanofiber-based myelination assays (Figures 5C–5F).

Confirmation of the hit compounds using rodent OPCs

Next, to assess if the effect of these compounds (Ro1138452 and SR2211) is specific only to human cells, we performed a validation experiment using purified primary mouse OPCs. The purified mouse OPCs treated with these molecules had significantly more MBP+ area compared to the DMSO treated culture (Figures 6A, 6B, S9A, and S9B). We also observed increased number of OLIG2+ cells in the culture treated with these molecules, which suggests that these compounds promote proliferation of the OL lineage cells in rodent OPCs (Figure 6D). No significant OPC proliferation, however, was observed in the hESC-derived OPC culture treated with these molecules. To confirm that the increased MBP+ area is not merely due to cell proliferation, we normalized MBP+ area to the number of OLIG2+ cells and show that the compounds significantly promote OPC to OL maturation in a dose dependent manner (Figures 6D, S9B, and S9C).

Single cell RNAseq of differentiating cultures treated with hit compounds

To better understand the transcripts and pathways modulated by the three small molecules (Ro1138452 and SR2211, and Ro25-6981 maleate), we next performed single cell transcriptomic analysis (scRNAseq) on a mixed population of differentiating OPC cultures that were treated either with DMSO or with one of the three small molecules of interest for 10 days. After removing potential doublets and cells with more than 20% mitochondrial gene content, a combined total of 18,713 cells were used for further analysis (Figures S10 and S11A, detail in STAR Methods section). Unsupervised clustering of the single cell transcripts from the combined dataset identified 15 distinct cell populations. Label prediction of the single cell clusters based on previously published datasets[13,29] and expression of marker genes, predicted three cycling progenitors (CyPs), an OPC, a pre-OL, an OL, a neuron-like, a pericyte, and five astrocyte (AS) cell populations (Figures 7B and S11B, Table S2). In addition, we identified two cell populations at transitional states that did not show enrichment of any specific maker gene sets (Figures 7E and S11C). Psuedotime and trajectory analysis indicate that the cells in this transitional state are potentially transitioning from

Table 1. List of top 15 hit compounds from each library

Molecule ID	Chemical name	Action	Biological Activity
JHMI-0110651	Oxiconazole	inhibitor	antifungal, inhibits of fungal cyctochrome P450 51 and inhibits ergosterol biosynthesis,
JHMI-0000208	Fluphenazine dihydrochloride	Antagonist	D1/D2 selective dopamine receptor antagonist
JHMI-0002272	Raloxifene hydrochloride	Modulator	Selective estrogen receptor modulator (SERM)
JHMI-0001917	Tetraisopropyl pyrophosphoramide	Inhibitor	Selective inhibitor of butyrylcholinesterase
JHMI-0000185	Clotrimazole	Inhibitor	Antifungal and Cytochrome P450 inhibitor; also, an inhibitor of the Ca2+-activated K+ channel
JHMI-0001683	Ro 25–6981 hydrochloride	Antagonist	NR2B-selective NMDA antagonist
JHMI-0110506	I-BET 151 dihydrochloride	Inhibitor	BET bromodomain inhibitor; also promotes differentiation of hiPSCs into megakaryocytes
JHMI-0000665	CARBETAPENTANE	Ligand	Opioid and sigma1 ligand
JHMI-0002181	ML-7	Inhibitor	Selective myosin light-chain kinase (MLCK) inhibitor
JHMI-0002388	(S)-(+)-Camptothecin	Inhibitor	DNA topoisomerase I inhibitor
JHMI-0002427	13-cis-retinoic acid, Isotretinoin	Regulator	Anti-inflammatory and antitumor actions mediated through RAR-beta and RAR-alpha receptors
JHMI-0000672	Tamoxifen citrate	Inhibitor	An anti-estrogen, Estrogen receptor partial agonist/antagonist
JHMI-0001554	Phosphoramidon disodium	Inhibitor	Inhibitor of mammalian enkephalinase and some metallo-endopeptidases; potent inhibitor of thermolysin and other bacterial metallo-endopeptidases
JHMI-0000623	Tretinoin	Activator	Exerts its effects by binding to nuclear retinoic acid receptors (RARs) which directly regulate gene expression
JHMI-0002272	Raloxifene hydrochloride	Modulator	Selective estrogen receptor modulator (SERM)
JHMI-0124771	ZK 200775	Antagonist	Competitive AMPA/kainate antagonist
JHMI-0124993	Ro 1,138,452 hydrochloride	Antagonist	Selective prostacyclin IP receptor antagonist
JHMI-0001683	Ro 25–6981 hydrochloride	Antagonist	NR2B-selective NMDA antagonist
JHMI-0125109	SR 2211	Agonist	Selective RORgamma inverse agonist
JHMI-0110506	I-BET 151 dihydrochloride	Inhibitor	BET bromodomain inhibitor; also promotes differentiation of hiPSCs into megakaryocytes
JHMI-0125334	SGC-CBP30	Inhibitor	Potent CBP/p300 BRD inhibitor
JHMI-0125143	ME 0328	Inhibitor	Selective PARP-3 inhibitor
JHMI-0125424	DG 172 dihydrochloride	inverse agonist	Potent PPARbeta/delta inverse agonist; promotes BMC differentiation
JHMI-0125008	JHW 007 hydrochloride	Antagonist	High affinity dopamine uptake inhibitor
JHMI-0001736	PNU 37883 hydrochloride	blocker	Vascular Kir6 (KATP) channel blocker
JHMI-0001980	TMPH hydrochloride	Inhibitor	Neuronal nicotinic receptor antagonist
JHMI-0125155	GSK 1562590 hydrochloride	Antagonist	High affinity, selective urotensin II (UT) receptor antagonist
JHMI-0125255	XMD 8-87	Inhibitor	Potent Ack1/TNK2 inhibitor

The first 15 compounds are from the LOPAC, and the last 15 are from the TOCRIS library of molecules.

progenitor state toward either neuron-like or astrocyte cells (Figures 7D and S11D). The trajectory analysis showed a linear path from CyPs to OL differentiation; however, the astrocyte cells in our differentiation culture seem to arise either from the CyPs or, similar to our previous report,[13] a sub-population of OPCs could also differentiate into astrocytes (Figure 7D).

We observed both the OL and Pre-OL cell proportion and average expression of OL marker genes (*MBP, PLP1, MAG, MOG*) in the OL cluster were slightly increased in the drug treated samples compared to the

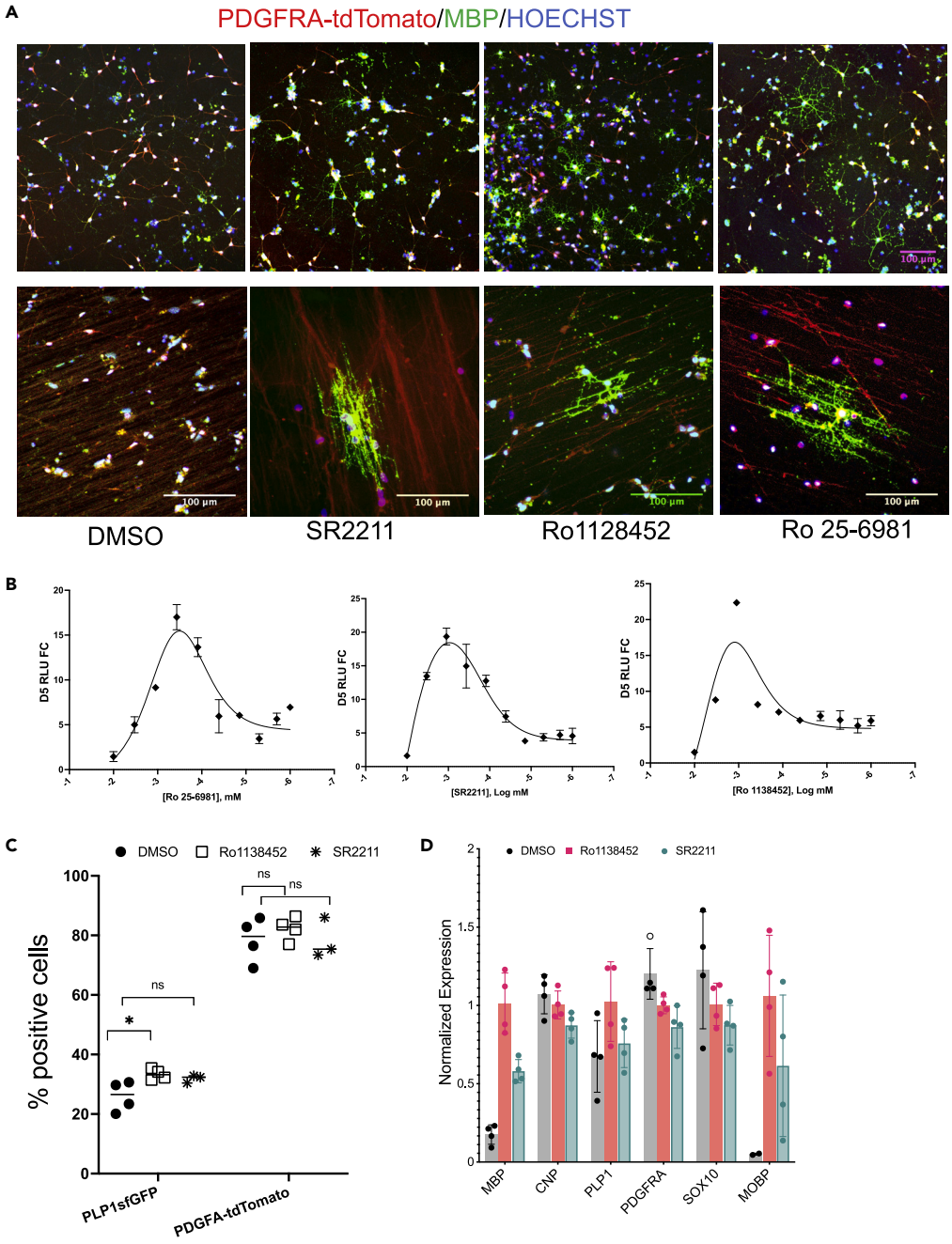

Figure 4. Validation of the promising hit compounds

(A) Immunostaining of purified OPCs treated with different compounds for 10 days show stronger MBP staining and more MBP+ cells (top panel) and appearance of improved myelination of electrospun nanofibers ((950 nM diameter nanofibers) lower panel) compared to the DMSO treated cells. Red channel was overexposed to visualize the nanofibers in the lower panel. Immunostaining was independently repeated three times with similar results; scale bar: 100 µm.

(B) MBP-Nanoluc activity in the PTt-P1-MsNL OPCs treated with different concentration of small molecules. Yaxis is the Nanoluc reading after 5 days of drug treatment, presented as fold change to day 0. Data presented as mean ± SEM.

(C and D) Flow analysis (C) and qPCR-based quantification (D) of the OPCs treated with different small molecules show increased number of PLP1-GFP+ cells and increased *PLP1* and other OL marker transcripts compared to the DMSO treated cells. In (C), comparison to DMSO is made using multiple unpaired t-test (*, P <0.05). Data for (D) is presented as mean ±SD.

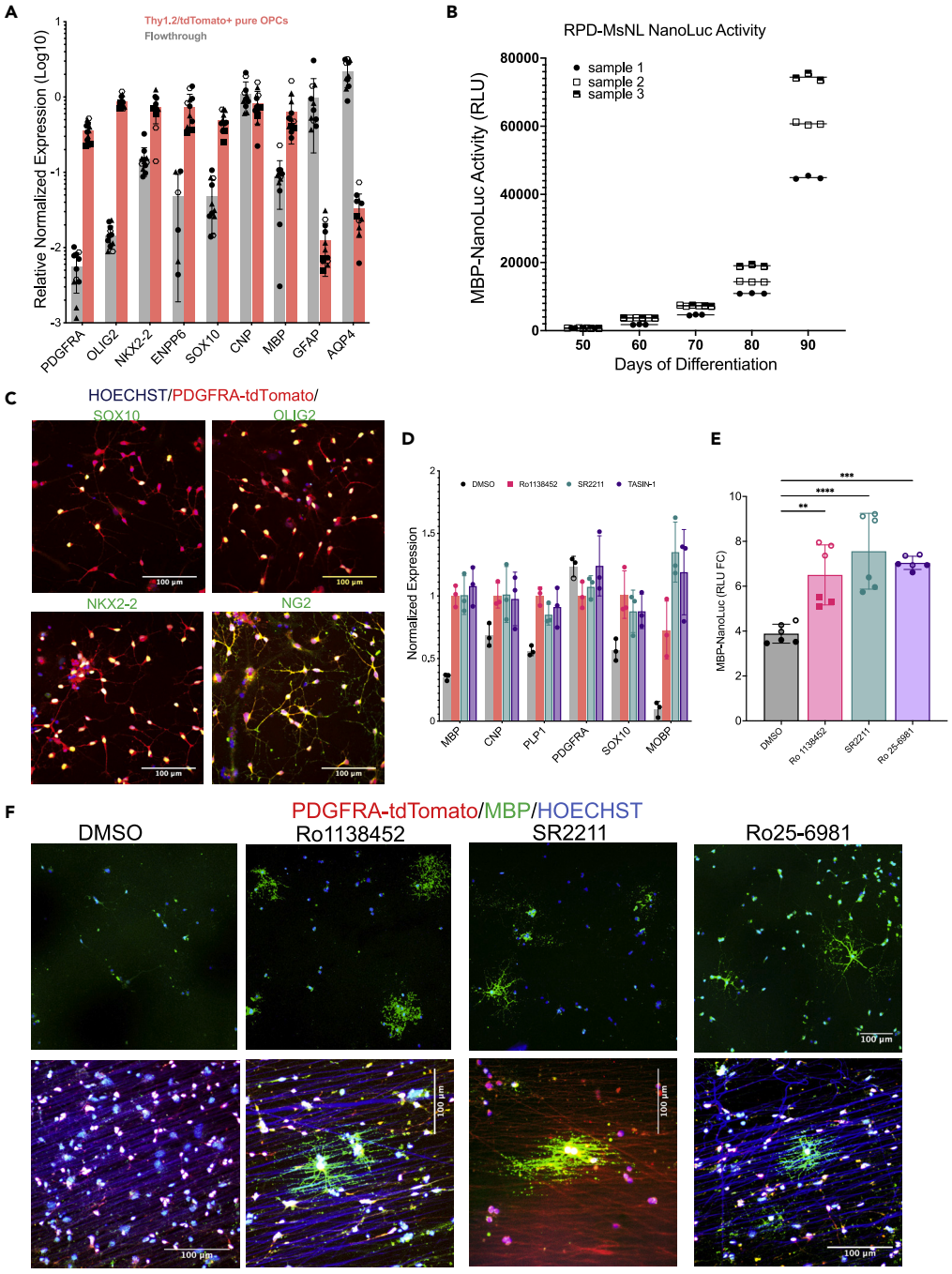

Figure 5. Validation of reporter OPCs generated using an independent, male hESC line (RUES1)

(A) Differentiated OPCs were MACS purified for the expression of PDGFRA-tdTomato-thy1.2, and the expression of different OPC markers between the tdTomato+ and tdTomato- (flow through) population were quantified by qPCR analysis, which shows enrichment of OPC markers in the tdTomato enriched population compared to the flow through. Three biological and three technical replicates each were used for qPCR analysis. Data are presented as mean ± SD. Biological and technical replicates are distinguished by filled vs clear symbols used for each data point. Source data for the qPCR are provided as a Source Data file.

(B) secNluc activity in the cell culture medium of differentiating RPD-MsNL reporter line measured with Nano-Glo assay. 20 µL of culture media from different days of differentiation (x-axis) were removed for the assay. Increase in Nano-Luc activity (y-axis), which corresponds to MBP expression increases as cells mature.

Figure 5. *Continued*

(C) Immunohistochemistry demonstrating that the MACS purified tdTomato+ cells express the OPC markers *SOX10, OLIG2, NKX2.2* and *NG2*. Immunohistochemistry was independently repeated three times with similar results.
(D-F) qPCR (D), NanoLuc expression (E), and immunostaining (F) of the purified RPD-MsNL OPCs treated with different compounds for 10 days. (E) NanoLuc data represents two different experiments performed using different number of OPCs, represented as open (10K cells per treatment) versus filled (20k cells per treatment) symbol. (F) Stronger MBP staining, more MBP+ cells (top panel) and better myelination of the electrospun nanofibers ((950 nM diameter nanofibers) lower panel) by the compound treated OPCs compared to the DMSO treated cells is noticeable. Red channel was overexposed to visualize the nanofibers in the lower panel. Immunostaining was independently repeated three times with similar results. Data are presented as mean ± SD, scale bar: 100 μm.

DMSO control (Figures 7G, 7H, and S10). Ro1138452 and Ro25-6981 treatment increased the OL and pre-OL cell proportion by 2-fold, but no increase was observed in the SR2211 treated samples. Ro25-6981 treatment also increased the proportion of OPC and CYP3 populations (Figure S10C), which have very high expression of OPC marker genes (Figures 7E and S11C). Average expression of the OL marker genes, particularly *MBP* and *MAG* was increased by Ro1138452 and SR2211, but not by Ro25-6981. We also observed reduction of astrocyte cell proportion in the drug treated samples. The proportion of AS1 and AS2 cell population was reduced in Ro1138452 and Ro 25–6981 treated samples, and the proportion of AS4 and AS5 was reduced in the SR2211 and Ro 25–6981 treated samples respectively (Figure 7, Table S3). These data suggest that: (1) SR2211 promotes the expression of OL marker genes but it might not significantly increase the proportion of the OL cell population, and (2) the increased proportion of OL cells in Ro1138452 and Ro25-6981 treated samples could potentially be at the expense of astrocyte lineage cells.

Gene set enrichment analysis reveals pathways modulated in OPCs and OLLCs by the drug treatments

We next identified the genes that are differentially expressed (DE) in the OL and OPC clusters of the drug treated samples compared to DMSO treated samples and performed gene set enrichment analysis (GSEA) on the differentially expressed genes. The GSEA revealed increased expression of genes related to sterol and cholesterol biosynthesis pathways (CBP) in the OL cluster of all the drug treated samples (Figure 8, Tables S4 and S5). CBP's role in OL maturation myelination has been previously reported.[11,30–32] A number of biological processes in the OL clusters that are unique to each drug treatment were also identified. Unfolded protein response (UPR) and ER stress pathways were enriched in the OL as well as OPC clusters of Ro1138452 and Ro25-6981 treated samples, but these pathways were significantly downregulated in the SR2211 treated cells (Figures 8A–8E). Processes associated with immune response such as antigen processing, regulation of Interleukin-8 and 1, complement activation, and response to interferon-gamma etc., were enriched in the SR2211 treated samples (Figure 8E). We also assessed the DE genes in OL lineage cells identified from the trajectory analysis (the Cyp > OP > pre-OL > OL trajectory) (Figure 7D) of drug treated samples when compared to the DMSO treatment. The majority of differentially expressed genes in the cells from this trajectory overlap between the samples (Figure 8F, Table S6). The highest number of unique DE genes was identified in the SR2211 treatment, and the GSEA analysis of these genes highlighted that the transport of insulin like growth factor (IGF), vascular endothelial growth factor A (VEGFA) signaling, and nuclear receptor (*NR1H3 and NR1H2*) mediated cholesterol transport are modulated by the SR2211 treatment (Figure 8G, Table S7).

Canonical target of the SR2211 and RO1138452

The known targets of SR2211 and RO1138452 are RORγ (RORC) and prostacyclin receptor (PTGIR), respectively. Of interest, the transcriptomic analysis showed that the canonical targets of both compounds were expressed at a very low level in the differentiating cells (Figure 8H). *PTGIR* expression was more abundant in the OL lineage cells than the astrocytes, and higher expression was detected in the OPCs and its expression is reduced in the OL population. This suggests that the inhibition of the IP receptor pathway by Ro1138452 could promote maturation of OPCs to OL. In contrast, very few cells in the differentiating culture express RORC, which suggests that SR2211 could be promoting OL differentiation by acting through a non-canonical pathway.

DISCUSSION

Promoting remyelination of neurons in the CNS is a promising approach for treatment of MS and other demyelinating neurodegenerations. If endogenous OPCs could be stimulated to differentiate and

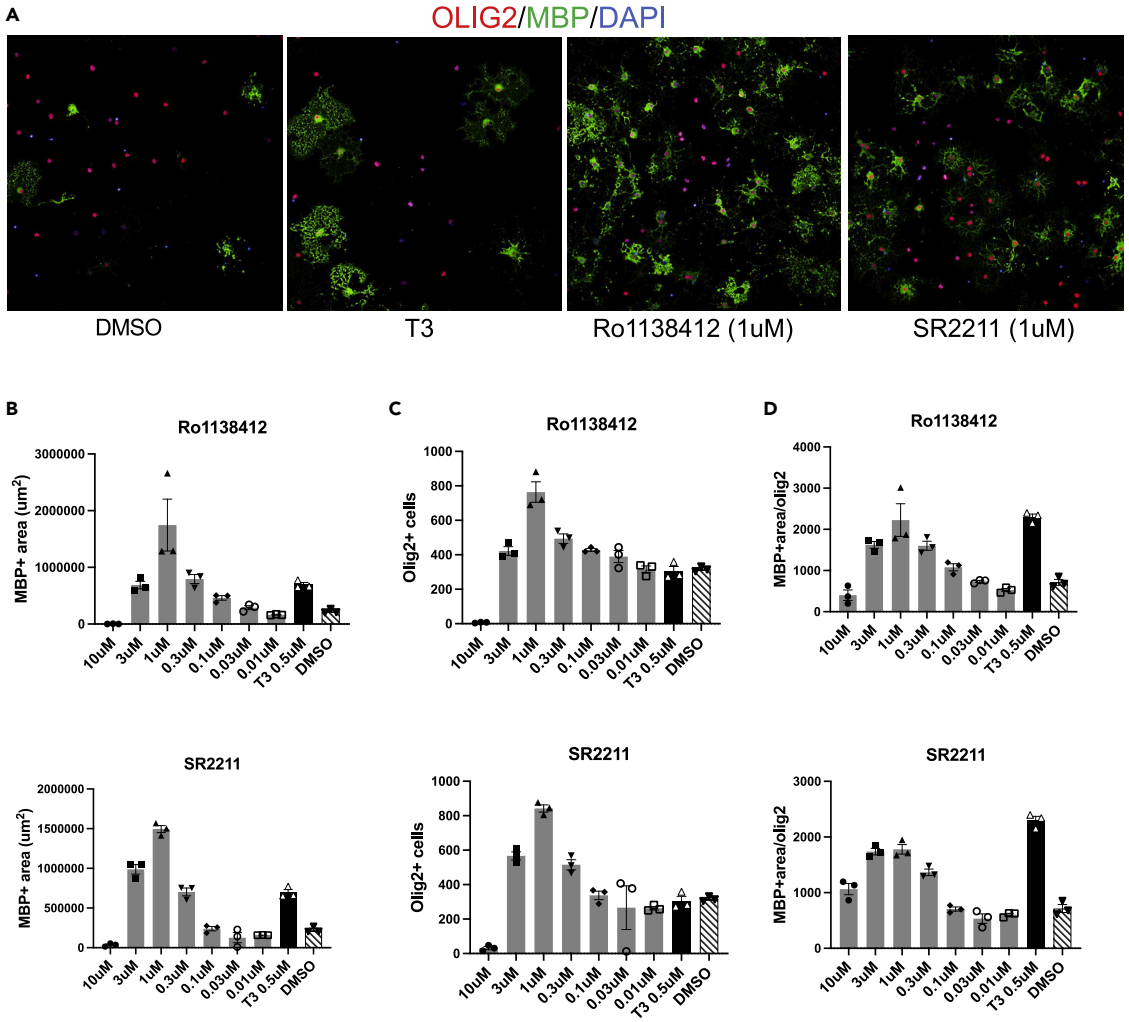

Figure 6. Ro1138412 and SR2211 promote differentiation of rodent OPCs

OPCs from P7-8 mice were purified using Anti-O4 microbeads and MACS purification method, and the purified OPCs were treated with one of the following molecules: Ro1138412, SR2211, T3 as positive control or DMSO.

(A) Immunostaining for MBP protein shows significant increase in MBP positive cells and MBP+ area in the drug treated samples.

(B–D) Quantification of MBP+ area (B) OLIG2+ cell number (C), and the MBP+ area relative to OLIG2+ cells in Ro1138412 treatment (top panels) and SR2211 treatment (bottom panels) compared to T3 and DMSO treatments. Data presented as mean ± SEM.

remyelinate affected axons, we could reduce and potentially stop disease progression, including the neurodegeneration aspects of the diseases, and might even be able to reverse already established disability in MS patients. Remyelination-based therapy could complement current immune-modulation-based treatments. Therefore, identification of lead small molecules that can promote differentiation of myelinogenic OPCs can have direct translational implications.

The systems being used currently to screen for drugs that promote oligodendrocyte maturation and myelin production are predominantly based on rodent cell model systems. For developing effective remyelination-based therapies, validating and expanding the mouse studies to a human system is essential. In addition, drug discovery performed with human cells has a better likelihood to identify leads that will translate into effective treatments. However, a verified human OPCs/OLs-based drug discovery platform has not yet been reported, probably due, in large part, owing to the difficulty and challenges in obtaining a large quantity of pure primary glial cells for such work. Because the human stem cell-derived OPCs and OL now provide a powerful and versatile source of human cell culture systems for drug discovery, we set forth to establish a drug screening platform that uses hPSC-derived OPCs and OLs.

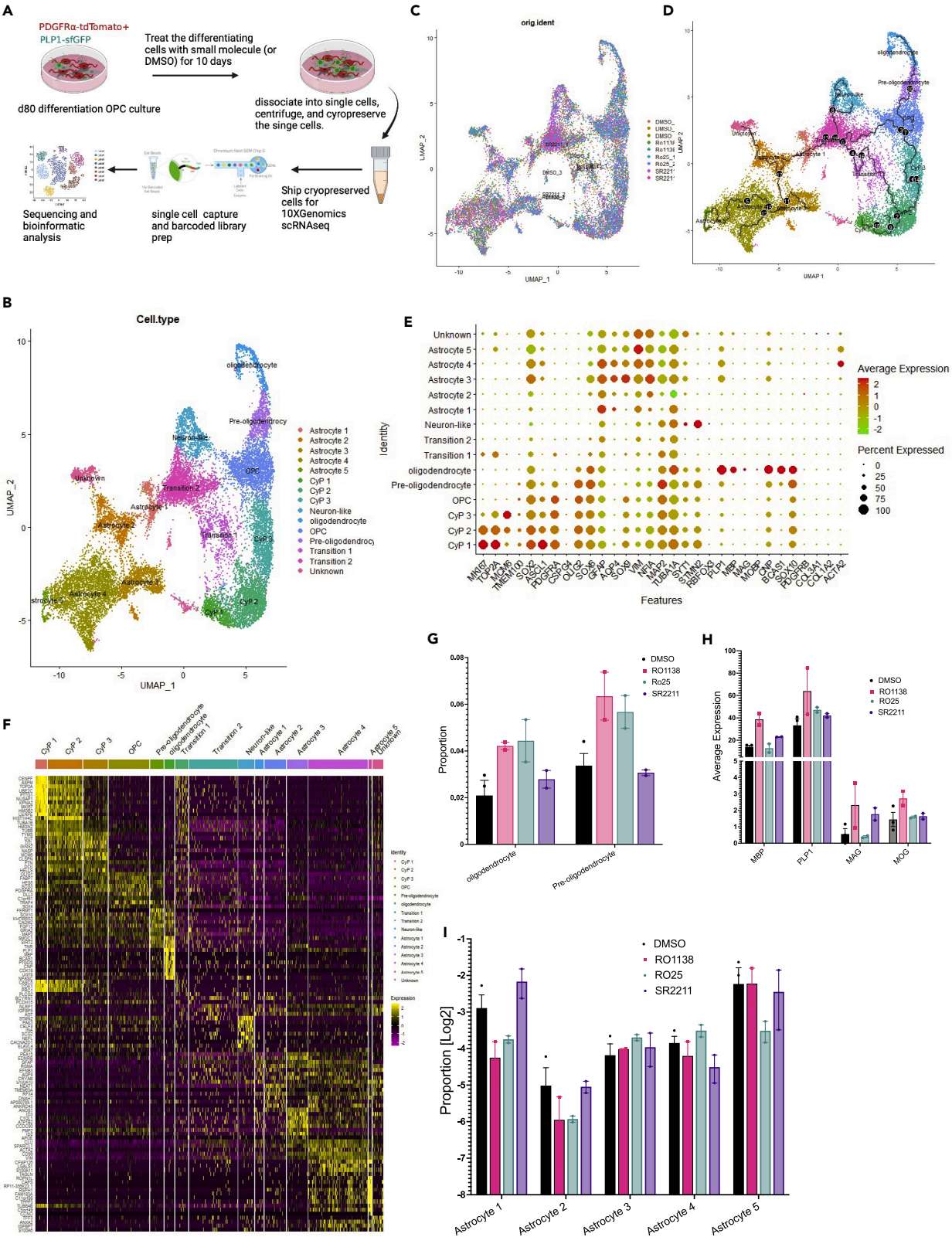
A
PDGFRα-tdTomato+
PLP1-sfGFP
Treat the differentiating cells with small molecule (or DMSO) for 10 days
d80 differentiation OPC culture
dissociate into single cells, centrifuge, and cryopreserve the singe cells.
Ship cryopreserved cells for 10XGenomics scRNAseq
single cell capture and barcoded library prep
Sequencing and bioinformatic analysis
B
Cell.type
UMAP_1
UMAP_2
Astrocyte 1
Astrocyte 2
Astrocyte 3
Astrocyte 4
Astrocyte 5
CyP 1
CyP 2
CyP 3
Neuron-like
oligodendrocyte
OPC
Pre-oligodendrocyte
Transition 1
Transition 2
Unknown
C
orig.ident
D
E
Identity
Features
Average Expression
Percent Expressed
F
Expression
G
Proportion
DMSO
RO1138
Ro25
SR2211
H
Average Expression
MBP
PLP1
MAG
MOG
I
Proportion [Log2]
Astrocyte 1
Astrocyte 2
Astrocyte 3
Astrocyte 4
Astrocyte 5

Figure 7. Single cell transcriptomic analysis of the differentiating PtP1MsNL OPCs treated with different small molecules

(A) schematic of the scRNAseq experiment. Day 80 differentiating OPCs were treated with small molecules for ten days before dissociation, single cell capture, and sequencing.

(B) Unsupervised clustering of the single cell transcriptional profiles of combined dataset including all the DMSO and drug treated samples. Cells are visualized with an UMAP embedding. The unbiased clustering divided the cell into 15 clusters.

(C) UMAP projection to visualize overlay of cells with different drug treatments.

(D) Trajectory analysis illustrating the maturation of mitotic progenitor cells to OL and astrocytes. Astrocytes seem to originate from early progenitors as well as OPCs.

(E) A dot plot showing average expression of a subset of known marker genes (Xaxis) across different clusters (Yaxis).

(F) heatmap of the top 10 enriched genes from each cluster. Yellow color represents increased expression.

(G and I) Proportion of cells in the oligodendrocyte and pre-oligodendrocytes clusters (G) and astrocyte clusters (I) between different drug treated samples.

(H) Average expression of oligodendrocyte markers genes in the OL cluster. Data in (G-I) are presented as mean ± SEM

We engineered a human embryonic stem cell-based reporter system with three reporters where two fluorescent proteins and secreted Nano luciferase (secNluc) protein are driven by OPC and OL specific promoters, and used OPCs derived from the reporter hESC to establish a drug screening platform that allows for high-throughput screening of myelination promoting drugs. With the secreted Nluc system, cells do not need to be sacrificed for analysis, allowing time-course studies and significant cost and research benefits. Using this system, we screened ~2500 bioactive molecules in at least two doses and three time-points. 240 potential hit compounds identified from an initial screen were further tested in duplicates at 7 doses and three-time points. The extensive data on the effect of these compounds on MBP protein expression in human OLs would not have been possible without the reporter system described here. Furthermore, the reporter cell system that we have established is suitable for a larger scale, human cell-based screen of remyelination compounds.

As a validation of our screening platform, several of the compounds we identified, including muscarinic receptor antagonists (benztropine, clemastine and carbetapentane) cytochrome P450 inhibitors (clotrimazole, oxiconazole), SERMs (raloxifene, tamoxifen), dopamine receptor antagonists (fluphenazine), and ROCK inhibitors (ML9, ML7) (Table 1) were recently reported as promoting remyelination of rodent OPCs.[9,11,16,33–35] In addition, inhibition of bromodomain containing proteins has been reported to help improve myelination in a murine system[22,23] but its role in the human system has not been examined. Tetraisopropyl pyrophosphoramide, an inhibitor of butyrylcholinesterase (BChE), is another compound of interest that was identified in our screen. A role of BChE in modulating neuroinflammation, demyelination, and neuropathology in MS has been suggested[21,36–38] and an inhibitor of BChE, rivastigmine, has been shown to suppress neuroinflammation in EAE models.[37] Our study provides validation of these targets in promoting OL differentiation in human OPC and OL system.

Possibly because of the use of the highly sensitive Nluc reporter system and also because we used human OPCs for our screens, given that it is well known that human and rodent cells differ in many important ways, we were able to identify a number of targets that have not been previously reported. We show that at least two of these new compounds identified from our screen increase OL maturation in the OPCs derived from two different hESC lines. Using the *in vitro* myelination assay that we have established, we found that these compounds could potentially promote myelination as well.

One of the compounds that we identified, Ro1138452, is a known inhibitor of the IP receptor (encoded by *PTGIR* gene). *PTGIR* is detected in the OL lineage cells in our scRNAseq dataset. The *PTGIR* transcript expression was higher in the OPCs and reduced in the OL population, which suggests that the inhibition of the IP receptor pathway by Ro1138452 could potentially promote maturation of OPCs to OL. PTGIR is also reported to be expressed by PDGFRA+ OPCs and PDGFRB+ pericyte cells in the mouse CNS and also in the PDGFRA+ cells in the CNS of MS patients.[39,40] Of interest, administration of Ro1138452 in the lysophosphatidylcholine (LPC) injected demyelination mouse model reduced the OPCs recruitment and impaired remyelination in the spinal cord.[39] It is possible that the IP pathway is essential for OPC migration to an injury site, but once the OPCs are recruited, repression of the IP pathway promotes OL maturation and myelination. Another possibility is that the IP pathway has species-specific different functions. Conditional loss of PTGIR function in mouse OPCs versus OL, and loss of PTGIR function in hPSC-derived OPCs/OL would assist in making the species-specific distinction and would also help to understand the role of IP pathway in OPC migration, OPC to OL maturation, and myelination.

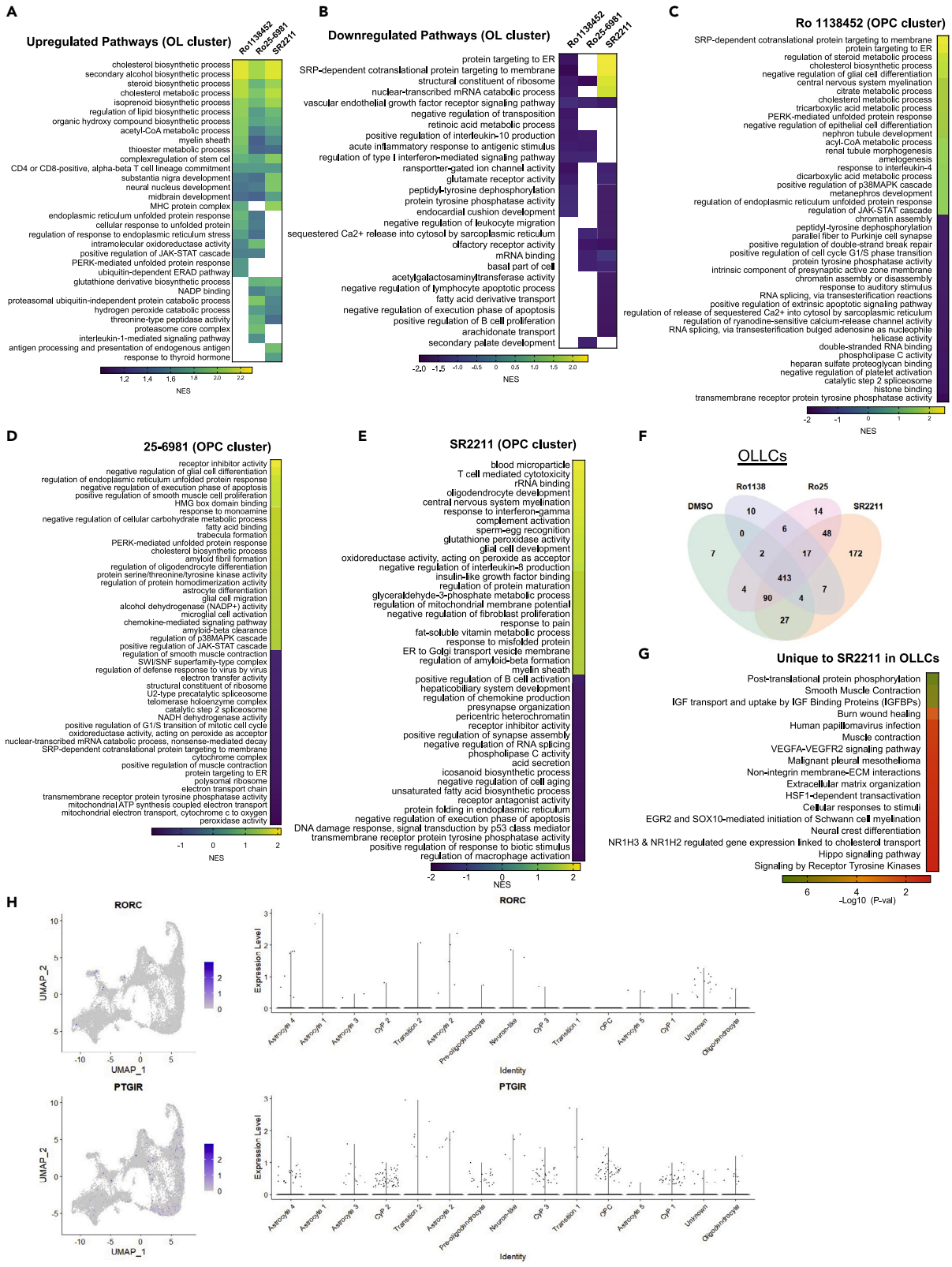
A
Upregulated Pathways (OL cluster)
Ro1138452
Ro25-6981
SR2211
cholesterol biosynthetic process
secondary alcohol biosynthetic process
steroid biosynthetic process
cholesterol metabolic process
isoprenoid biosynthetic process
regulation of lipid biosynthetic process
organic hydroxy compound biosynthetic process
acetyl-CoA metabolic process
myelin sheath
thioester metabolic process
complexregulation of stem cel
CD4 or CD8-positive, alpha-beta T cell lineage commitment
substantia nigra development
neural nucleus development
midbrain development
MHC protein complex
endoplasmic reticulum unfolded protein response
cellular response to unfolded protein
regulation of response to endoplasmic reticulum stress
intramolecular oxidoreductase activity
positive regulation of JAK-STAT cascade
PERK-mediated unfolded protein response
ubiquitin-dependent ERAD pathway
glutathione derivative biosynthetic process
NADP binding
proteasomal ubiquitin-independent protein catabolic process
hydrogen peroxide catabolic process
threonine-type peptidase activity
proteasome core complex
interleukin-1-mediated signaling pathway
antigen processing and presentation of endogenous antigen
response to thyroid hormone
1.2 1.4 1.6 1.8 2.0 2.2
NES
B
Downregulated Pathways (OL cluster)
Ro1138452
Ro25-6981
SR2211
protein targeting to ER
SRP-dependent cotranslational protein targeting to membrane
structural constituent of ribosome
nuclear-transcribed mRNA catabolic process
vascular endothelial growth factor receptor signaling pathway
negative regulation of transposition
retinoic acid metabolic process
positive regulation of interleukin-10 production
acute inflammatory response to antigenic stimulus
regulation of type I interferon-mediated signaling pathway
ransporter-gated ion channel activity
glutamate receptor activity
peptidyl-tyrosine dephosphorylation
protein tyrosine phosphatase activity
endocardial cushion development
negative regulation of leukocyte migration
sequestered Ca2+ release into cytosol by sarcoplasmic reticulum
olfactory receptor activity
mRNA binding
basal part of cell
acetylgalactosaminyltransferase activity
negative regulation of lymphocyte apoptotic process
fatty acid derivative transport
negative regulation of execution phase of apoptosis
positive regulation of B cell proliferation
arachidonate transport
secondary palate development
-2.0 -1.5 -1.0 -0.5 0 0.5 1.0 1.5 2.0
NES
C
Ro 1138452 (OPC cluster)
SRP-dependent cotranslational protein targeting to membrane
protein targeting to ER
regulation of steroid metabolic process
cholesterol biosynthetic process
negative regulation of glial cell differentiation
central nervous system myelination
citrate metabolic process
cholesterol metabolic process
tricarboxylic acid metabolic process
PERK-mediated unfolded protein response
negative regulation of epithelial cell differentiation
nephron tubule development
acyl-CoA metabolic process
renal tubule morphogenesis
amelogenesis
response to interleukin-4
dicarboxylic acid metabolic process
positive regulation of p38MAPK cascade
metanephros development
regulation of endoplasmic reticulum unfolded protein response
regulation of JAK-STAT cascade
chromatin assembly
peptidyl-tyrosine dephosphorylation
parallel fiber to Purkinje cell synapse
positive regulation of double-strand break repair
positive regulation of cell cycle G1/S phase transition
protein tyrosine phosphatase activity
intrinsic component of presynaptic active zone membrane
chromatin assembly or disassembly
response to auditory stimulus
RNA splicing, via transesterification reactions
positive regulation of extrinsic apoptotic signaling pathway
regulation of release of sequestered Ca2+ into cytosol by sarcoplasmic reticulum
regulation of ryanodine-sensitive calcium-release channel activity
RNA splicing, via transesterification bulged adenosine as nucleophile
helicase activity
double-stranded RNA binding
phospholipase C activity
heparan sulfate proteoglycan binding
negative regulation of platelet activation
catalytic step 2 spliceosome
histone binding
transmembrane receptor protein tyrosine phosphatase activity
-2 -1 0 1 2
NES
D
25-6981 (OPC cluster)
receptor inhibitor activity
negative regulation of glial cell differentiation
regulation of endoplasmic reticulum unfolded protein response
negative regulation of execution phase of apoptosis
positive regulation of smooth muscle cell proliferation
HMG box domain binding
response to monoamine
negative regulation of cellular carbohydrate metabolic process
fatty acid binding
trabecula formation
PERK-mediated unfolded protein response
cholesterol biosynthetic process
amyloid fibril formation
regulation of oligodendrocyte differentiation
protein serine/threonine/tyrosine kinase activity
regulation of protein homodimerization activity
astrocyte differentiation
glial cell migration
alcohol dehydrogenase (NADP+) activity
microglial cell activation
chemokine-mediated signaling pathway
amyloid-beta clearance
regulation of p38MAPK cascade
positive regulation of JAK-STAT cascade
regulation of smooth muscle contraction
SWI/SNF superfamily-type complex
regulation of defense response to virus by virus
electron transfer activity
structural constituent of ribosome
U2-type precatalytic spliceosome
telomerase holoenzyme complex
catalytic step 2 spliceosome
NADH dehydrogenase activity
positive regulation of G1/S transition of mitotic cell cycle
oxidoreductase activity, acting on peroxide as acceptor
nuclear-transcribed mRNA catabolic process, nonsense-mediated decay
SRP-dependent cotranslational protein targeting to membrane
cytochrome complex
positive regulation of muscle contraction
protein targeting to ER
polysomal ribosome
electron transport chain
transmembrane receptor protein tyrosine phosphatase activity
mitochondrial ATP synthesis coupled electron transport
mitochondrial electron transport, cytochrome c to oxygen
peroxidase activity
-1 0 1 2
NES
E
SR2211 (OPC cluster)
blood microparticle
T cell mediated cytotoxicity
rRNA binding
oligodendrocyte development
central nervous system myelination
response to interferon-gamma
complement activation
sperm-egg recognition
glutathione peroxidase activity
glial cell development
oxidoreductase activity, acting on peroxide as acceptor
negative regulation of interleukin-8 production
insulin-like growth factor binding
regulation of protein maturation
glyceraldehyde-3-phosphate metabolic process
regulation of mitochondrial membrane potential
negative regulation of fibroblast proliferation
response to pain
fat-soluble vitamin metabolic process
response to misfolded protein
ER to Golgi transport vesicle membrane
regulation of amyloid-beta formation
myelin sheath
positive regulation of B cell activation
hepaticobiliary system development
regulation of chemokine production
presynapse organization
pericentric heterochromatin
receptor inhibitor activity
positive regulation of synapse assembly
negative regulation of RNA splicing
phospholipase C activity
acid secretion
icosanoid biosynthetic process
negative regulation of cell aging
unsaturated fatty acid biosynthetic process
receptor antagonist activity
protein folding in endoplasmic reticulum
negative regulation of execution phase of apoptosis
DNA damage response, signal transduction by p53 class mediator
transmembrane receptor protein tyrosine phosphatase activity
positive regulation of response to biotic stimulus
regulation of macrophage activation
-2 -1 0 1 2
NES
F
OLLCs
Ro1138
Ro25
DMSO
SR2211
10
14
0
6
48
7
2
17
172
413
4
7
90
4
27
G
Unique to SR2211 in OLLCs
Post-translational protein phosphorylation
Smooth Muscle Contraction
IGF transport and uptake by IGF Binding Proteins (IGFBPs)
Burn wound healing
Human papillomavirus infection
Muscle contraction
VEGFA-VEGFR2 signaling pathway
Malignant pleural mesothelioma
Non-integrin membrane-ECM interactions
Extracellular matrix organization
HSF1-dependent transactivation
Cellular responses to stimuli
EGR2 and SOX10-mediated initiation of Schwann cell myelination
Neural crest differentiation
NR1H3 & NR1H2 regulated gene expression linked to cholesterol transport
Hippo signaling pathway
Signaling by Receptor Tyrosine Kinases
6 4 2
-Log10 (P-val)
H
RORC
UMAP_2
UMAP_1
Expression Level
Astrocyte 4
Astrocyte 1
Astrocyte 3
OPC 2
Transition 2
Astrocyte 2
Pre-oligodendrocyte
Neuron-like
OPC 3
Transition 1
OPC
Astrocyte 5
OPC 1
Unknown
Oligodendrocyte
Identity
PTGIR

Figure 8. Gene set enrichment analysis of the small molecule treated samples when compared to DMSO treatment

(A and B) Heatmaps of GSEA to show few highlighted pathways that are upregulated (A) or downregulated (B) in the OL cluster of different drugs treated samples.

(C–E) Up or downregulated pathways in the OPC cells treated with different small molecules. Detailed GSEA for all the clusters are listed in supplemental data X.

(F) Venn diagram showing overlap of genes enriched in the cells within OLLC trajectory (Figure 7D) of different drug treated samples.

(G) Heatmap of GSEA analysis highlighting few pathways that are enriched in the OLLCs of SR2211 treated samples. GSEA was performed with the 172 enriched genes that are unique to the SR2211 treatment.

(H) Expression of RORC and PTGIR, canonical targets of SR2211 and Ro1138452 in the single cell RNAseq dataset.

Another compound that we identified, SR2211, which has been shown to specifically inhibit RORγ,[41] was a very interesting finding because of the well-known function RORγ in regulating immune homeostasis. Specifically, the RORγt isoform of RORγ is crucial for differentiation of Th17 cells and the expression of Interleukin 17 (IL-17)[42–44] which has been implicated in the pathology of multiple sclerosis (MS).[45,46] Prevention of IL-17 production both by genetic ablation RORC and by pharmacological inhibition of RORγ[44] is shown to protect mice from developing experimental autoimmune encephalomyelitis (EAE), a mouse model of MS.[43] However, a direct role of RORγ inhibition in promoting myelination had not been previously documented. Of note, ursolic acid (UA), which is known to promote remyelination, is also a potent RORy inhibitor, but UA is reported to act via PPARγ activation.[47] Because SR2211 is known to specifically target RORγ, our data suggests that modulation of RORγ pathway could benefit inflammatory demyelination such as MS by both immune modulation and remyelination. Pro-myelinating effect of RORγ inhibition is particularly interesting because numerous reports have suggested that cholesterol biosynthesis intermediates (CBIs), especially those between lanosterol and zymosterol that promote OL maturation and myelination,[11] have been reported to act as ligands to RORγ and modulate its activity.[48–50] Therefore, it is possible that the RORγ is the not yet identified link that connects cholesterol biosynthesis to OL differentiation and myelination. On the other hand, because only a handful of cells in our differentiating OPC/OL culture express RORC, it is possible that SR2211 is working through a non-canonical pathway or by its off-target effect on RORA, PPARγ or androgen receptor.[51] Alternatively, SR2211 working via a non-cell autonomous manner by targeting astrocyte cells is also possible. The ongoing loss of RORC function in human iPSC-derived OPCs/OL/astrocytes should help us better understand the role of RORγ in OL maturation and myelination, define their target pathways, and investigate their therapeutic potential.

Limitations of the study

We have established a robust human cell-based drug screening platform for the discovery of pro-myelinating compounds, performed a small-scale proof-of-principle drug screen, and identified a number of promising compounds. Current limitations of the study are that the genetic validation of the pathways targeted by these small molecules and *in vivo* testing of the molecules in rodent models of demyelination have not been performed. These studies would help to improve our understanding of the activity of these molecules.

STAR★METHODS

Detailed methods are provided in the online version of this paper and include the following:

- KEY RESOURCES TABLE
- RESOURCE AVAILABILITY
  - Lead contact
  - Material availability
  - Data and code availability
- EXPERIMENTAL MODEL AND SUBJECT DETAILS
  - Human pluripotent stem cells (PSCs) and culture conditions
  - Primary mouse OPCs
- METHOD DETAILS
  - Cloning
  - Generation of reporter cell lines
  - Oligodendrocyte differentiation protocol
  - Flow cytometry and MACS purification of the reporter hOPCs
  - Nanofiber-based myelination assay
  - qRT-PCR, immunofluorescence staining, and microscopy

- High-throughput screening
- *In vitro* mouse OPC culture, drug treatment, and imaging
- Single-cell transcriptomic analysis

- QUANTIFICATION AND STATISTICAL ANALYSIS

SUPPLEMENTAL INFORMATION

Supplemental information can be found online at https://doi.org/10.1016/j.isci.2023.106156.

ACKNOWLEDGMENTS

Funding: Grants from the Gilbert Family Foundation (DJZ, XC), National Institutes of Health grants P30 EY001765 (DJZ, Wilmer Eye Institute), Sanofi Inc. (XC, DJZ), National Institutes of Health grants K99 EY029011 and R00EY029011 (XC), Unrestricted funds from Research to Prevent Blindness (Wilmer Eye Institute), and Generous gifts from the Guerrieri Family Foundation (DJZ).

AUTHOR CONTRIBUTIONS

W.L. assisted with experimental designs, conducted experiments, conducted bioinformatic analysis, and edited the manuscript. C.B. assisted with experimental design and high-throughput screening assay and analysis. Y.H., G.S., S.M., and J.C.D. assisted with the screening and RNA work. F.T., X.C., and Y.D. assisted in generating the stem cell reporters and differentiation of hESC-derived OPCs. W.F., C.C., and H.J., assisted with bioinformatic analysis. D.J.Z. designed the study, edited the manuscript, and provided funding support. X.C. designed the study, performed experiments, wrote the manuscript, and provided funding support.

DECLARATION OF INTERESTS

D.J.Z. and X.C. are inventors on an intellectual property disclosure related to the technology described in the manuscript that has been filed with Johns Hopkins University, which seeks to license the technology.

INCLUSION AND DIVERSITY

We support inclusive, diverse, and equitable conduct of research.

Received: August 1, 2022
Revised: October 18, 2022
Accepted: February 3, 2023
Published: February 8, 2023

REFERENCES

1. Franklin, R.J.M. (2002). Why does remyelination fail in multiple sclerosis? Nat. Rev. Neurosci. *3*, 705–714. https://doi.org/10.1038/nrn917.

2. Pietrangelo, A. (2014). Multiple Sclerosis by the Numbers: Facts, Statisctics, and You (Healthiline Networks, Inc).

3. Levine, J.M., and Reynolds, R. (1999). Activation and proliferation of endogenous oligodendrocyte precursor cells during ethidium bromide-induced demyelination. Exp. Neurol. *160*, 333–347. https://doi.org/10.1006/exnr.1999.7224.

4. Penderis, J., Shields, S.A., and Franklin, R.J.M. (2003). Impaired remyelination and depletion of oligodendrocyte progenitors does not occur following repeated episodes of focal demyelination in the rat central nervous system. Brain *126*, 1382–1391.

5. Franklin, R.J.M., and Ffrench-Constant, C. (2008). Remyelination in the CNS: from biology to therapy. Nat. Rev. Neurosci. *9*, 839–855. https://doi.org/10.1038/nrn2480.

6. Chang, A., Tourtellotte, W.W., Rudick, R., and Trapp, B.D. (2002). Premyelinating oligodendrocytes in chronic lesions of multiple sclerosis. N. Engl. J. Med. *346*, 165–173. https://doi.org/10.1056/NEJMoa010994.

7. Peppard, J.V., Rugg, C.A., Smicker, M.A., Powers, E., Harnish, E., Prisco, J., Cirovic, D., Wright, P.S., August, P.R., and Chandross, K.J. (2015). High-content phenotypic screening and triaging strategy to identify small molecules driving oligodendrocyte progenitor cell differentiation. J. Biomol. Screen *20*, 382–390. https://doi.org/10.1177/1087057114559490.

8. Mei, F., Fancy, S.P.J., Shen, Y.A.A., Niu, J., Zhao, C., Presley, B., Miao, E., Lee, S., Mayoral, S.R., Redmond, S.A., et al. (2014). Micropillar arrays as a high-throughput screening platform for therapeutics in multiple sclerosis. Nat. Med. *20*, 954–960. https://doi.org/10.1038/nm.3618.

9. Najm, F.J., Madhavan, M., Zaremba, A., Shick, E., Karl, R.T., Factor, D.C., Miller, T.E., Nevin, Z.S., Kantor, C., Sargent, A., et al. (2015). Drug-based modulation of endogenous stem cells promotes functional remyelination in vivo. Nature *522*, 216–220. https://doi.org/10.1038/nature14335.

10. Elitt, M.S., Barbar, L., and Tesar, P.J. (2018). Drug screening for human genetic diseases using iPSC models. Hum. Mol. Genet. *27*, R89–R98. https://doi.org/10.1093/hmg/ddy186.

11. Hubler, Z., Allimuthu, D., Bederman, I., Elitt, M.S., Madhavan, M., Allan, K.C., Shick, H.E., Garrison, E., T Karl, M., Factor, D.C., et al. (2018). Accumulation of 8,9-unsaturated sterols drives oligodendrocyte formation and remyelination. Nature *560*, 372–376. https://doi.org/10.1038/s41586-018-0360-3.

12. Mei, F., Mayoral, S.R., Nobuta, H., Wang, F., Desponts, C., Lorrain, D.S., Xiao, L., Green, A.J., Rowitch, D., Whistler, J., and Chan, J.R. (2016). Identification of the kappa-opioid receptor as a therapeutic target for oligodendrocyte remyelination. J. Neurosci. *36*, 7925–7935. https://doi.org/10.1523/JNEUROSCI.1493-16.2016.

13. Chamling, X., Kallman, A., Fang, W., Berlinicke, C.A., Mertz, J.L., Devkota, P., Pantoja, I.E.M., Smith, M.D., Ji, Z., Chang, C., et al. (2021). Single-cell transcriptomic reveals molecular diversity and developmental heterogeneity of human stem cell-derived oligodendrocyte lineage cells. Nat. Commun. *12*, 652. https://doi.org/10.1038/s41467-021-20892-3.

14. Sluch, V.M., Chamling, X., Liu, M.M., Berlinicke, C.A., Cheng, J., Mitchell, K.L., Welsbie, D.S., and Zack, D.J. (2017). Enhanced stem cell differentiation and immunopurification of genome engineered human retinal ganglion cells. Stem Cells Transl. Med. *6*, 1972–1986. https://doi.org/10.1002/sctm.17-0059.

15. Kim, J.H., Lee, S.R., Li, L.H., Park, H.J., Park, J.H., Lee, K.Y., Kim, M.K., Shin, B.A., and Choi, S.Y. (2011). High cleavage efficiency of a 2A peptide derived from porcine teschovirus-1 in human cell lines, zebrafish and mice. PLoS One *6*, e18556. https://doi.org/10.1371/journal.pone.0018556.

16. Nadeem, M., and Sloane, J.A. (2015). Targeting remyelination treatment for multiple sclerosis. World J. Neurol. *5*, 5. https://doi.org/10.5316/wjn.v5.i1.5.

17. Stangel, M., Kuhlmann, T., Matthews, P.M., and Kilpatrick, T.J. (2017). Achievements and obstacles of remyelinating therapies in multiple sclerosis. Nat. Rev. Neurol. *13*, 742–754. https://doi.org/10.1038/nrneurol.2017.139.

18. Melchor, G.S., Khan, T., Reger, J.F., and Huang, J.K. (2019). Remyelination pharmacotherapy investigations highlight diverse mechanisms underlying multiple sclerosis progression. ACS Pharmacol. Transl. Sci. *2*, 372–386. https://doi.org/10.1021/acsptsci.9b00068.

19. Reale, M., Costantini, E., Di Nicola, M., D'Angelo, C., Franchi, S., D'Aurora, M., Di Bari, M., Orlando, V., Galizia, S., Ruggieri, S., et al. (2018). Butyrylcholinesterase and Acetylcholinesterase polymorphisms in Multiple Sclerosis patients: implication in peripheral inflammation. Sci. Rep. *8*, 1319. https://doi.org/10.1038/s41598-018-19701-7.

20. Fields, R.D., Dutta, D.J., Belgrad, J., and Robnett, M. (2017). Cholinergic signaling in myelination. Glia *65*, 687–698. https://doi.org/10.1002/glia.23101.

21. Darvesh, S., Leblanc, A.M., Macdonald, I.R., Reid, G.A., Bhan, V., Macaulay, R.J., and Fisk, J.D. (2010). Butyrylcholinesterase activity in multiple sclerosis neuropathology. Chem. Biol. Interact. *187*, 425–431. https://doi.org/10.1016/j.cbi.2010.01.037.

22. Gacias, M., Gerona-Navarro, G., Plotnikov, A.N., Zhang, G., Zeng, L., Kaur, J., Moy, G., Rusinova, E., Rodriguez, Y., Matikainen, B., et al. (2014). Selective chemical modulation of gene transcription favors oligodendrocyte lineage progression. Chem. Biol. *21*, 841–854. https://doi.org/10.1016/j.chembiol.2014.05.009.

23. Chiang, C.M. (2014). Nonequivalent response to bromodomain-targeting BET inhibitors in oligodendrocyte cell fate decision. Chem. Biol. *21*, 804–806. https://doi.org/10.1016/j.chembiol.2014.07.003.

24. Krasnow, A.M., and Attwell, D. (2016). NMDA receptors: power switches for oligodendrocytes. Neuron *91*, 3–5. https://doi.org/10.1016/j.neuron.2016.06.023.

25. Káradóttir, R., Cavelier, P., Bergersen, L.H., and Attwell, D. (2005). NMDA receptors are expressed in oligodendrocytes and activated in ischaemia. Nature *438*, 1162–1166. https://doi.org/10.1038/nature04302.

26. De Biase, L.M., Kang, S.H., Baxi, E.G., Fukaya, M., Pucak, M.L., Mishina, M., Calabresi, P.A., and Bergles, D.E. (2011). NMDA receptor signaling in oligodendrocyte progenitors is not required for oligodendrogenesis and myelination. J. Neurosci. *31*, 12650–12662. https://doi.org/10.1523/JNEUROSCI.2455-11.2011.

27. Elitt, M.S., Shick, H.E., Madhavan, M., Allan, K.C., Clayton, B.L.L., Weng, C., Miller, T.E., Factor, D.C., Barbar, L., Nawash, B.S., et al. (2018). Chemical screening identifies enhancers of mutant oligodendrocyte survival and unmasks a distinct pathological phase in pelizaeus-merzbacher disease. Stem Cell Rep. *11*, 711–726. https://doi.org/10.1016/j.stemcr.2018.07.015.

28. Douvaras, P., Wang, J., Zimmer, M., Hanchuk, S., O'Bara, M.A., Sadiq, S., Sim, F.J., Goldman, J., and Fossati, V. (2014). Efficient generation of myelinating oligodendrocytes from primary progressive multiple sclerosis patients by induced pluripotent stem cells. Stem Cell Rep. *3*, 250–259. https://doi.org/10.1016/j.stemcr.2014.06.012.

29. Jäkel, S., Agirre, E., Mendanha Falcão, A., van Bruggen, D., Lee, K.W., Knuesel, I., Malhotra, D., Ffrench-Constant, C., Williams, A., and Castelo-Branco, G. (2019). Altered human oligodendrocyte heterogeneity in multiple sclerosis. Nature *566*, 543–547. https://doi.org/10.1038/s41586-019-0903-2.

30. Ačimovič, J., Goyal, S., Košir, R., Goličnik, M., Perše, M., Belič, A., Urlep, Ž., Guengerich, F.P., and Rozman, D. (2016). Cytochrome P450 metabolism of the post-lanosterol intermediates explains enigmas of cholesterol synthesis. Sci. Rep. *6*, 28462. https://doi.org/10.1038/srep28462.

31. Hubler, Z., Friedrich, R.M., Sax, J.L., Allimuthu, D., Gao, F., Rivera-León, A.M., Pleshinger, M.J., Bederman, I., and Adams, D.J. (2021). Modulation of lanosterol synthase drives 24,25-epoxysterol synthesis and oligodendrocyte formation. Cell Chem. Biol. *28*, 866–875.e5. https://doi.org/10.1016/j.chembiol.2021.01.025.

32. Khandker, L., Jeffries, M.A., Chang, Y.J., Mather, M.L., Evangelou, A.V., Bourne, J.N., Tafreshi, A.K., Ornelas, I.M., Bozdagi-Gunal, O., Macklin, W.B., and Wood, T.L. (2022). Cholesterol biosynthesis defines oligodendrocyte precursor heterogeneity between brain and spinal cord. Cell Rep. *38*, 110423. https://doi.org/10.1016/j.celrep.2022.110423.

33. Du, C., Duan, Y., Wei, W., Cai, Y., Chai, H., Lv, J., Du, X., Zhu, J., and Xie, X. (2016). Kappa opioid receptor activation alleviates experimental autoimmune encephalomyelitis and promotes oligodendrocyte-mediated remyelination. Nat. Commun. *7*, 11120. https://doi.org/10.1038/ncomms11120.

34. Dietz, K.C., Polanco, J.J., Pol, S.U., and Sim, F.J. (2016). Targeting human oligodendrocyte progenitors for myelin repair. Exp. Neurol. *283*, 489–500. https://doi.org/10.1016/j.expneurol.2016.03.017.

35. Lariosa-Willingham, K.D., Rosler, E.S., Tung, J.S., Dugas, J.C., Collins, T.L., and Leonoudakis, D. (2016). Development of a high throughput drug screening assay to identify compounds that protect oligodendrocyte viability and differentiation under inflammatory conditions. BMC Res. Notes *9*, 444. https://doi.org/10.1186/s13104-016-2219-8.

36. Lumsden, C.E. (1951). Fundamental problems in the pathology of multiple sclerosis and allied demyelinating diseases. Br. Med. J. *1*, 1035–1043. https://doi.org/10.1136/bmj.1.4714.1035.

37. Lumsden, C.E. (1952). Quantitative studies on lipolytic enzyme activity in degenerating and regenerating nerve. Q. J. Exp. Physiol. Cogn. Med. Sci. *37*, 45–57. https://doi.org/10.1113/expphysiol.1952.sp000979.

38. Kim, S.U., Oh, T., and Johnson, D.D. (1972). Developmental changes of acetylcholinesterase and pseudocholinesterase in organotypic cultures of spinal cord. Exp. Neurol. *35*, 274–281. https://doi.org/10.1016/0014-4886(72)90153-7.

39. Takahashi, C., Muramatsu, R., Fujimura, H., Mochizuki, H., and Yamashita, T. (2013). Prostacyclin promotes oligodendrocyte precursor recruitment and remyelination after spinal cord demyelination. Cell Death Dis. *4*, e795. https://doi.org/10.1038/cddis.2013.335.

40. Muramatsu, R., Kuroda, M., Matoba, K., Lin, H., Takahashi, C., Koyama, Y., and Yamashita, T. (2015). Prostacyclin prevents pericyte loss and demyelination induced by lysophosphatidylcholine in the central nervous system. J. Biol. Chem. *290*, 11515–11525. https://doi.org/10.1074/jbc.M114.587253.

41. Kumar, N., Lyda, B., Chang, M.R., Lauer, J.L., Solt, L.A., Burris, T.P., Kamenecka, T.M., and Griffin, P.R. (2012). Identification of SR2211: a potent synthetic RORgamma-selective modulator. ACS Chem. Biol. *7*, 672–677. https://doi.org/10.1021/cb200496y.

42. Ruan, Q., Kameswaran, V., Zhang, Y., Zheng, S., Sun, J., Wang, J., DeVirgiliis, J., Liou, H.C., Beg, A.A., and Chen, Y.H. (2011). The Th17

immune response is controlled by the Rel-RORgamma-RORgamma T transcriptional axis. J. Exp. Med. *208*, 2321–2333. https://doi.org/10.1084/jem.20110462.

43. Yang, X.O., Pappu, B.P., Nurieva, R., Akimzhanov, A., Kang, H.S., Chung, Y., Ma, L., Shah, B., Panopoulos, A.D., Schluns, K.S., et al. (2008). T helper 17 lineage differentiation is programmed by orphan nuclear receptors ROR alpha and ROR gamma. Immunity *28*, 29–39. https://doi.org/10.1016/j.immuni.2007.11.016.

44. Solt, L.A., Kumar, N., Nuhant, P., Wang, Y., Lauer, J.L., Liu, J., Istrate, M.A., Kamenecka, T.M., Roush, W.R., Vidović, D., et al. (2011). Suppression of TH17 differentiation and autoimmunity by a synthetic ROR ligand. Nature *472*, 491–494. https://doi.org/10.1038/nature10075.

45. Kang, Z., Wang, C., Zepp, J., Wu, L., Sun, K., Zhao, J., Chandrasekharan, U., DiCorleto, P.E., Trapp, B.D., Ransohoff, R.M., and Li, X. (2013). Act1 mediates IL-17-induced EAE pathogenesis selectively in NG2+ glial cells. Nat. Neurosci. *16*, 1401–1408. https://doi.org/10.1038/nn.3505.

46. Wang, C., Zhang, C.J., Martin, B.N., Bulek, K., Kang, Z., Zhao, J., Bian, G., Carman, J.A., Gao, J., Dongre, A., et al. (2017). IL-17 induced NOTCH1 activation in oligodendrocyte progenitor cells enhances proliferation and inflammatory gene expression. Nat. Commun. *8*, 15508. https://doi.org/10.1038/ncomms15508.

47. Zhang, Y., Li, X., Ciric, B., Curtis, M.T., Chen, W.J., Rostami, A., and Zhang, G.X. (2020). A dual effect of ursolic acid to the treatment of multiple sclerosis through both immunomodulation and direct remyelination. Proc. Natl. Acad. Sci. USA *117*, 9082–9093. https://doi.org/10.1073/pnas.2000208117.

48. Santori, F.R., Huang, P., van de Pavert, S.A., Douglass, E.F., Jr., Leaver, D.J., Haubrich, B.A., Keber, R., Lorbek, G., Konijn, T., Rosales, B.N., et al. (2015). Identification of natural RORgamma ligands that regulate the development of lymphoid cells. Cell Metab. *21*, 286–298. https://doi.org/10.1016/j.cmet.2015.01.004.

49. Jetten, A.M., Takeda, Y., Slominski, A., and Kang, H.S. (2018). Retinoic acid-related Orphan Receptor gamma (RORgamma): connecting sterol metabolism to regulation of the immune system and autoimmune disease. Curr. Opin. Toxicol. *8*, 66–80. https://doi.org/10.1016/j.cotox.2018.01.005.

50. Jetten, A.M., and Cook, D.N. (2020). Inverse) agonists of retinoic acid-related orphan receptor gamma: regulation of immune responses, inflammation, and autoimmune disease. Annu. Rev. Pharmacol. Toxicol. *60*, 371–390. https://doi.org/10.1146/annurev-pharmtox-010919-023711.

51. Wang, J., Zou, J.X., Xue, X., Cai, D., Zhang, Y., Duan, Z., Xiang, Q., Yang, J.C., Louie, M.C., Borowsky, A.D., et al. (2016). ROR-gamma drives androgen receptor expression and represents a therapeutic target in castration-resistant prostate cancer. Nat. Med. *22*, 488–496. https://doi.org/10.1038/nm.4070.

52. Schindelin, J., Arganda-Carreras, I., Frise, E., Kaynig, V., Longair, M., Pietzsch, T., Preibisch, S., Rueden, C., Saalfeld, S., Schmid, B., et al. (2012). Fiji: an open-source platform for biological-image analysis. Nat. Methods *9*, 676–682. https://doi.org/10.1038/nmeth.2019.

53. Wu, T., Hu, E., Xu, S., Chen, M., Guo, P., Dai, Z., Feng, T., Zhou, L., Tang, W., Zhan, L., et al. (2021). clusterProfiler 4.0: a universal enrichment tool for interpreting omics data. Innovation *2*, 100141. https://doi.org/10.1016/j.xinn.2021.100141.

54. Sluch, V.M., Chamling, X., Wenger, C., Duan, Y., Rice, D.S., and Zack, D.J. (2018). Highly efficient scarless knock-in of reporter genes into human and mouse pluripotent stem cells via transient antibiotic selection. PLoS One *13*, e0201683. https://doi.org/10.1371/journal.pone.0201683.

55. Douvaras, P., and Fossati, V. (2015). Generation and isolation of oligodendrocyte progenitor cells from human pluripotent stem cells. Nat. Protoc. *10*, 1143–1154. https://doi.org/10.1038/nprot.2015.075.

56. Chambers, S.M., Fasano, C.A., Papapetrou, E.P., Tomishima, M., Sadelain, M., and Studer, L. (2009). Highly efficient neural conversion of human ES and iPS cells by dual inhibition of SMAD signaling. Nat. Biotechnol. *27*, 275–280. https://doi.org/10.1038/nbt.1529.

57. Ren, Y.J., Zhang, S., Mi, R., Liu, Q., Zeng, X., Rao, M., Hoke, A., and Mao, H.Q. (2013). Enhanced differentiation of human neural crest stem cells towards the Schwann cell lineage by aligned electrospun fiber matrix. Acta Biomater. *9*, 7727–7736. https://doi.org/10.1016/j.actbio.2013.04.034.

58. Sluch, V.M., Davis, C.-h.O., Ranganathan, V., Kerr, J.M., Krick, K., Martin, R., Berlinicke, C.A., Marsh-Armstrong, N., Diamond, J.S., Mao, H.-Q., and Zack, D.J. (2015). Differentiation of human ESCs to retinal ganglion cells using a CRISPR engineered reporter cell line. Sci. Rep. *5*, 16595. https://doi.org/10.1038/srep16595.

59. Korsunsky, I., Millard, N., Fan, J., Slowikowski, K., Zhang, F., Wei, K., Baglaenko, Y., Brenner, M., Loh, P.R., and Raychaudhuri, S. (2019). Fast, sensitive and accurate integration of single-cell data with Harmony. Nat. Methods *16*, 1289–1296. https://doi.org/10.1038/s41592-019-0619-0.

60. Stuart, T., Butler, A., Hoffman, P., Hafemeister, C., Papalexi, E., Mauck, W.M., 3rd, Hao, Y., Stoeckius, M., Smibert, P., and Satija, R. (2019). Comprehensive integration of single-cell data. Cell *177*, 1888–1902.e21. https://doi.org/10.1016/j.cell.2019.05.031.

61. Trapnell, C. (2016). Monocole: differential expression and time-series analysis for single-cell RNA-Se. http://cole-trapnell-lab.github.io/monocle-release/articles/v2.2.0.

STAR★METHODS

KEY RESOURCES TABLE

REAGENT or RESOURCE	SOURCE	IDENTIFIER
Antibodies		
Anti-PDGFR alpha	R&D Systems	AF-307-SP
PE anti-human CD140a (PDGFRalpha)	BioLegend	323505
Anti-SOX10	R&D Systems	AF2864-SP
Anti-NKX2.2	DSHB	Cat# 74.5A5; RRID:AB_531794
Anti-MBP	Millipore	Cat# MAB386; RRID:AB_94975
Anti-OLIG2	Millipore	Cat# AB9610, RRID:AB_570666
Anti-O4 clone 81	Millipore	MAB345
Hoechst 33342	ThermoFisher Scientific	H3570
Alexa Fluor 488 goat anti-rabbit IgG	ThermoFisher Scientific	A-11034
Alexa Fluor 488 goat anti-mouse IgM	ThermoFisher Scientific	A-21042
Alexa Fluor 647 goat anti-rabbit IgG	ThermoFisher Scientific	A-21245
Alexa Fluor 647 donkey anti-goat IgG	ThermoFisher Scientific	A-21447
Bacterial and virus strains		
DH10B	ThermoFisher Scientific	C404010
Chemicals, peptides, and recombinant proteins		
mTeSR1	Stem Cell Technologies	5850
StemFlex	ThermoFisher Scientific	A3349401
DMEM/F12	ThermoFisher Scientific	11320082
Accutase	ThermoFisher Scientific	A11105-01
Antibiotic-Antimycotic	ThermoFisher Scientific	15240062
Growth Factor Reduced BD MatrigelTM Matrix	BD Biosciences	354230
Blebbistatin	Sigma	B0560-1MG
Opti-MEM™ I Reduced Serum Medium	ThermoFisher Scientific	31985088
CryoStor® CS10	Stem Cell Technologies	7930
CTLC-ABC	Immunospot	NC9711917
Lipofectamine™ Stem Transfection Reagent	ThermoFisher Scientific	STEM00001
Puromycin	ThermoFisher Scientific	A11138-03
N2 supplement	ThermoFisher Scientific	17502-048
B27 Supplement without vitamin A	ThermoFisher Scientific	12587-010
SB431542	Stem Cell Technologies	72234
LDN193189	Stem Cell Technologies	72147
Smoothened agonist	Sigma	R2625
All-trans retinoic acid	Millipore	566660
Recombinant human PDGF-AA	R&D Systems	221-AA-050
Recombinant human IGF-I	R&D Systems	291-G1-200
Recombinant human HGF	R&D Systems	294-HG-025
Neurotrophin 3 (NT3)	Millipore	GF031
cAMP analog	Sigma	D0260
3,3,5-Triiodo-l-thyronine (T3)	Sigma	T2877

(*Continued on next page*)

Continued

REAGENT or RESOURCE	SOURCE	IDENTIFIER
l-Ascorbic acid	Sigma	A4403
Insulin solution human	Sigma	19278
Biotin	Sigma	4639
Poly-L-ornithine hydrobromide	Sigma	3655
HEPES (1 M)	ThermoFisher Scientific	15630080
Laminin	MilliporeSigma	L2020-1MG
Critical commercial assays		
MycoAlert Mycoplasma Detection kit	Lonza	LT07-218
hPSC Genetic Analysis Kit	StemCell Technologies	7550
Nano-Glo® Luciferase Assay System	Promega	N1120
Neural Tissue Dissociation Kit	Miltenyi	130-092-628
Deposited data		
Single cell RNAseq	This study	Database: GSE223599
Human single cell data	Chamling et al.,[13] Jakel et al.[29]	GEO Database: (GSE118257, GSE104276 GSE146373), Bioproject (544731))
Human reference genome NCBI build 37, GRCh37	Genome Reference Consortium	http://www.ncbi.nlm.nih.gov/projects/genome/assembly/grc/human/
Experimental models: Cell lines		
Passage 40 hESC (WA09) or H9 NIH HES # 0062	WiCell	RRID:CVCL_9773
Passage 26 hESC (RUES1)	WiCell	RRID:CVCL_B809
PTt-P1-MsNL (the triple reporter)	This paper	N/A
Oligonucleotides		
Primers for Reporter Cell line (see Table S8)	This paper	N/A
qPCR Primers (see Table S8)	This paper	N/A
Recombinant DNA		
PX459.V2	Addgene	RRID:Addgene_62988
ZeroBlunt TOPO	ThermoFisher Scientific	K280020
MBP-P2A-secNanoluc	This paper	N/A
PLP1-sfGFP	This paper	N/A
Software and algorithms		
ImageJ	Schneider et al.[52]	https://imagej.net/software/fiji/
GraphPad Prism, V9	GraphPad Software, LLC	https://www.graphpad.com
CFX Maestro	Biorad	12004128
Harmony software 4.9	Perkin Elmer	HH17000010
Cellomics CX7	ThermoFisher Scientific	HCSDCX7LEDPRO
R package	Wu et al.[53]	ClusterProfiler

RESOURCE AVAILABILITY

Lead contact

Further information and requests for resources and reagents should be directed to and will be fulfilled by the lead contact, Xitiz Chamling (xchamli1@jhmi.edu).

Material availability

Materials are available upon request.

Data and code availability

- Raw data for all the compounds screened in our system is uploaded as Table S1.
- scRNAseq data is uploaded to NCBI gene expression repository (GSE223599).
- No new codes were generated for this study.
- Any additional information required to analyze the data reported in this study will be made available by the lead contact upon request.

EXPERIMENTAL MODEL AND SUBJECT DETAILS

Human pluripotent stem cells (PSCs) and culture conditions

hESC WA09 and RUES1 (both WiCell), NIH-approved hESC lines (NIH approval number: NIHhESC-10-0062, and 0012), were used for this study. All hESCs related experiments were conducted by following all policies and regulations established by the Johns Hopkins University Embryonic Stem Cell Research Oversight committee. hESCs were maintained in mTesr or mTesr plus (85,850 or 100–0276, Stem Cell Technologies) on growth factor-reduced Matrigel (354,230, Corning) coated plates at 37C, 10% CO2/5% O2. hPSC colonies were passaged by dissociating with Accutase (A6964, Sigma-Aldrich). Cells were maintained in stem cell media containing 5 mM blebbistatin (B0560, Sigma-Aldrich) for the first 24 hours after passaging, to improve single cell survival. Karyotype analysis was performed using a qPCR based hPSC Genetic Analysis Kit (StemCell Technologies, #07550) and KaryoStat Karyotyping (ThermoFisher). Chromosomal Cells were routinely tested for mycoplasma contamination (MycoAlert, Lonza) and only the cells free of contamination were used for OPC differentiation.

Primary mouse OPCs

To test the effect of our two compounds on mouse OPCs, brain tissues from postnatal day 7–8 (P7-8) C57Bl/6 mice of mixed sex were collected. All animal experiments were performed at Sanofi's animal facilities, a fully accredited Association for Assessment and Accreditation of Laboratory Animal Care facilities, by following the protocols approved by the Sanofi Institutional Animal Care and Use Committee Animals.

METHOD DETAILS

Cloning

A guide sequence targeting the stop codon of the *MBP and PLP1* locus was designed in Deskgen.com. Guide sequence with minimal off target and very high activity score was chosen and cloned into the BbsI restriction site of the Cas9 plasmid (Cas9-P2A-Puro modified from Addgene #62988[54]). pSpCas9(BB)-2A-Puro (PX459) V2.0 was a gift from Feng Zhang (Addgene plasmid # 62988; http://n2t.net/addgene:62988). To clone the donor plasmid, a ~2 kb PCR product was amplified from genomic DNA extracted from H9 ES cells and cloned into Zero Blunt TOPO cloning vector (ThermoFisher Scientific) to create an intermediate donor plasmid. Either the P2A-secNanoLuc or the sfGFP reporter DNA sequence was then introduced into the intermediate donor plasmid, precisely upstream of either the *MBP* or *PLP1* stop codon, using Gibson assembly (New England Biolabs). NanoLuc plasmids were purchased from Promega. Plasmid maps and sequences used for cloning are included in Table S8.

Generation of reporter cell lines

Method for gene editing and report cell line generation, previously reported by our lab,[13,14,52] was followed. Cells were transfected using the Lipofectamine Stem (STEM00001, ThermoFisher Scientific) transfection reagent following the manufacturer's recommended protocol. 0.35 μg Cas9 plasmid containing a gRNA sequence and 0.75 μg of donor plasmid were used for transfection. Two days after the transfection, the cells were selected with 750 ng/mL of puromycin for 24 hours, washed and cultured for 5 more days in the same dish with daily media change. After 5 days, the surviving cells were passaged at 500–1000 single cells per well of a 6 well plate for picking individual colonies and PCR-based genotyping.[54] PCR was performed using the Phusion Flash mastermix (ThermoFisher Scientific) and a 2-step PCR protocol following the manufacturer's instruction. Clones with clear homozygous knock-In were selected for the MBP-secNluc (Figures S1D andS1E), and a clone with heterozygous KI was chosen for the For PLP1-sfGFP reporter. For the PLP1-sfG KI clone, another allele of the PLP1 locus was sequenced to make sure that it had no mutation.

Oligodendrocyte differentiation protocol

Previously published and well-established oligodendrocyte differentiation protocol[55] was followed with minor modifications. Briefly, hESCs were dissociated to single cells and plated on Matrigel coated plate at 100,000 cells/well of a 6-well plate and maintained in mTesr plus at 37C, 10% CO2/5% O2. For RUES1 cells 200K cells were used to start differentiation. Two days after passaging, neural differentiation and spinal cord patterning was induced through dual SMAD inhibition (SB431542, 10uM and LDN193189, 250 nM) and 100 nM all-trans RA.[56] From day 8 to day 12, differentiating cells were maintained in neural induction media supplemented with RA (100 nM) and SAG (1 mM). At day 12, adherent cells were lifted and cultured in low-attachment plates to favor sphere aggregation. At day 30, spheres were plated into poly-L-ornithine/laminin-coated dishes in a media supplemented with, B27 (Thermo Fisher, 12587010), N2 supplement (Thermo Fisher, 17502048), PDGF-AA (221-AA-10, R&D systems), neurotrophin-3 (GF0308, MilliporeSigma), HGF (294-HG-025 R&D systems), Minocycline (Y0001930, Sigma) and T3 (T2877, Sigma).

Flow cytometry and MACS purification of the reporter hOPCs

For flow cytometry analysis and MACS purification, cells were dissociated into single cell suspension by incubating in accutase for ~45 minutes. The single cell suspension was then passed through a ~70 uM cell strainer (BD Biosciences), washed, and resuspended in Live Cell Imaging Solution (ThermoFisher Scientific) for flow analysis or MACS buffer (Miltenyi Biotec (Auburn, CA)) for MACS cell sorting. Flow analysis was performed with an SH800S Cell Sorter (Sony Biotechnology, San Jose, CA). BSC and FSC were used to select and subset live cells, and only live cells were used to quantify the number of tdTomato+ or GFP+ cells. A gate was set up using WT hES cells differentiated to day 95. MACS purification was performed by following manufacturer's instructions with minor modifications. Cells were resuspended in MACS buffer after passing through cell strainer. A CD90.2 (THY1.2) or O4 MicroBeads were added to the single cell suspension that is resuspended in MACS buffer and incubated at room temperature for 15 minutes for cell binding. Cells were run through the LS or MS magnetic column, columns were washed 3 times with the MACS buffer, and the cells bound to the column were recovered by pushing the cells through using a syringe provided. To increase the purity of tdTomato+ population, the cells collected from the column were run through a new column without additional supplementation of MicroBeads.

Nanofiber-based myelination assay

Aligned polycaprolactone (PCL) nanofibers were electrospun on a glass coverslip according to a previously reported method.[57,58] The average diameter of the fibers collected was 950 nm $\pm$ 200 nm. The nanofibers on coverslips were sterilized by soaking in 95% ethanol, and then washed three times with PBS. The nanofiber coverslips were placed on a 24 well plate and coated with PLO (50 μg/mL) for 4 hours followed by laminin (10 μg/mL) at 37°C overnight. Before cell seeding, laminin was aspirated and the coverslip was allowed to dry completely. For each well of a 24 well plate containing a nanofiber coverslip, 5000 purified OPCs were resuspended in 50 ul of PDGF media and the cells were added to the center of the coverslip. Cells were allowed to attach for 30 mins before gently adding 500 uL of the PDGF media/well to culture the cells. Media with small molecules or DMSO was replenished every 4–5 days. At the end of the experiment. media was removed, cells were fixed with 4% PFA, and used for immunofluoresce staining and imaging.

qRT-PCR, immunofluorescence staining, and microscopy

Total RNA was isolated using the RNeasy Mini Kit (QIAGEN) and reverse transcribed using the High-Capacity cDNA Reverse Transcription Kit (Applied Biosystems). A 2uL PCR reaction was set up using acoustic liquid handler (ECHO 550, Labcyte) and performed with the CFX384 real-time PCR instrument (Bio-Rad). Assays included at least three technical and two biological replicates unless otherwise stated, and were run using the Ssoadvanced Universal SYBR Green Supermix (Bio-Rad).

For immunofluorescence staining, cells were fixed with 4% paraformaldehyde, and simultaneously permeabilized and blocked with 0.2% Triton X-100 + 5% BSA +5% normal goat serum (or a serum specific to the host of secondary antibody) for an hour. Cells were then incubated with appropriate dilution of primary antibodies (Anti-PDGFR alpha (1:200); PE anti-human CD140a (1:100); Anti-SOX10 (1:100); Anti-NKX2.2 (1:50); Anti-MBP (1:100); Anti-OLIG2 (1:500); Anti-O4 (1:200)) overnight followed by secondary antibodies (Alexa Fluor 488/647 (1:500)) for 2 hours. Fluorescence images were taken using either the EVOS FL Auto 2 (ThermoFisher Scientific) or Zeiss 510 confocal microscope.

High-throughput screening

MACS purified reporter OPCs from day 75–85 differentiating culture was used for screening. 1.5K cells/well in of purified OPCs were plated in PLO-laminin coated 384 well plates using the EL406 (BioTeK) peristaltic liquid dispenser. 50uL of PDGF media was used per well to plate the cells. On the day of drug treatment (on day 2 after plating the cells) 20 uL of culture media was removed from each well using an integra ViaFlow 384, and Nluc activity in the media was measured (day 0 reading).

Nluc activity was measured using NanoGlo luciferase assay reagents (Promega N1150) following manufacturer's instruction with few modifications. 2.5 uL NanoGlo reaction mix was diluted with water (1:1 dilution) and the 5 uL diluted NanoGlo reaction mix was added per well containing 20uL of media. RLU reading was performed with a microplate reader (ClariOstar, BMG Labtech) using the preloaded settings for Nano luciferase and 0.1s exposure.

Drug dispensing was performed using ECHO 555, acoustic liquid handler. First, an intermediate plate with 10 uL of glial media in each well of a new sterile 384 well plate was prepared. Appropriate volume of small molecules was dispensed into each well using the ECHO. Since the highest dose (10 uM) was dispensed from the 10 mM stock solution, the maximum DMSO dose cells would receive was 0.01%, which is known to be well tolerated by cells *in vitro*. Additional 10 uL media was added to each well containing the small molecules. Using integra ViaFlow 384, 20 uL of the media containing small molecules was transferred from the intermediate plate to the plate containing cells. After adding the small molecules cells were cultured in 37 C, 5% Co2 incubator. Every 5 days, 20 uL of media was removed, Nluc activity measured and fresh media with small molecules was replenished as described above. On day 15, cells were fixed with 4% PFA, washed with PBS and either stored in 4C or immediately imaged using a High-Content Imager (Cellomics CX7).

In vitro mouse OPC culture, drug treatment, and imaging

Mouse OPC isolation, culture and treatment

C57Bl/6 mouse brains were collected on P7-8 and stored in Hibernate A (Thermofisher, A124750) medium until tissue digestion. The digestion was conducted using a Neural Tissue Dissociation Kit (Miltenyi, 130-092-628) and the gentalMACs Dissociator (Miltenyi) in accordance with the manufacturer's protocol. Anti-O4 microbeads (Miltenyi, 130-094-543) and LS columns (Miltenyi, 130-042-401) were used to positively select for OPCs per the manufacturer's protocol. The isolated cells were plated 10,000 cells per well on black 96-well plates (Perkin Elmer, 6055302), coated with 100 μg/mL Poly-D-lysine (Sigma, P6407) for at least 1 hour. Cells were cultured in DMEM/F12 (Gibco, 11330-057) with 1% N2 (Invitrogen,17502048), 100 U/ml Penicillin/100 μg/mL Streptomycin (Gibco, 15140122), 0.01% bovine serum albumin (Sigma, A9576), 5 μg/mL N-Acetyl-L-cysteine (Sigma, A8199), 10 ng/mL d-Biotin (Sigma, B4639), 2% B27 (Invitrogen, 17504044), 1 mM pyruvate (Gibco, 11360070), 5 μg/ml insulin (Sigma, I9278), 4.2 μg/mL forskolin (Sigma, F6886) and 10 ng/mL CNTF (Peprotech, 450-50). To promote proliferation, 20 ng/mL PDGF-AA (Invitrogen, PHG0035) and 1 ng/mL NT-3 (Peprotech, 450-03) were added to the medium. After two days, the proliferation medium was removed and replaced with differentiation medium (proliferation medium minus PDGF-AA and NT-3) and the Ro1138412 and SR2211 treatments were administered. Two days later the media was replenished. Cells were fixed in 4% PFA (Electron Microscopy Sciences, 15714S) three days later for a total of 5 days of treatment.

Mouse OPC immunostaining and imaging

Fixed cells were incubated with 10% normal goat serum (Vector Labs, S-1000) in PBS (Gibco, 10010023) with 0.2% Triton X-100 (Sigma, T9284; PBST) for 30 min to block nonspecific binding. The primary antibodies used were rat anti-myelin basic protein (BioRad, MCA409, 1:400 dilution) and rabbit anti-Olig2 (Millipore, AB9610 1:400). Cells were incubated with the primary antibodies in 5% normal goat serum in PBST overnight at 4C. The secondary antibodies used were AlexaFluor488 and AlexaFluor555 (1:1000, Invitrogen, A11006 and A21428), incubated for 1hr at room temperature. The cells were imaged on the Opera Phenix (Perkin Elmer). 21 images per well were taken with 4x1um thick Z Stack. Images were analyzed using Harmony software 4.9 (Perkin Elmer).

Single-cell transcriptomic analysis

Sample preparation

The reporter hESCs were differentiated to OPCs by following the protocol described above. On day 30 of differentiation, neurospheres were plated on a 6-well culture dish to facilitate OPC migration from the

plated spheres. 3 wells of day 80 differentiating cultures were treated DMSO as control and two wells each were treated with different small molecules for 10 days. Media with small molecules were replenished every three days. At the end of drug treatment, cells from each well were dissociated into single cells by treating with accutase for 45 minutes (just the cells that had migrated out from the spheres were collected, the spheres remain mostly intact). Single cells were passed through 40 uM cell strainers, washed once with PBS, cryopreserved in CTLC-ABC (NC9711917, Immunospot) buffer, and stored in −80 before shipping for single cell capture.

Single cell capture

The cryopreserved cells were thawed by following the instructions provided for CTLC-ABC. Cells were washed and counted on the DeNovex cell counter. Single cell capture, barcoding, post GEM-RT cleanup, cDNA amplification, and 3′ library construction was performed using the 10X genomics' single-cell RNA-seq technology by following their detailed instructions. Sequencing was performed on a Illumina Novaseq sequencer.

Quality control (QC) and clustering and differential gene expression

For quality control, only genes whose expression was detected in at least three cells were included in the analysis. To filter out potential doublets and poor cell samples, cells that had more than 7000 features or less than 250 features were excluded. We also excluded cells with more than 20% mitochondrial gene content. The remaining 18,714 cells that passed QC were used for all the downstream analysis. Log-normalization, principal component analysis (PCA), the Uniform Manifold Approximation and Projection (UMAP) were conducted using the Seurat package R. 2000 highly variable genes were used as input for PCA analysis. Samples from the different treatment groups were integrated using the Harmony package for R[59] to remove possible batch effects. A 30-dimensional reduction by harmony with resolution 0.5 was used for the UMAP embedding and clustering. To identify differentially expressed genes from each cluster, generalized linear regression in the MAST package was performed on the genes that are expressed in at least 10% of cells in each treatment group and have a minimum of 0.25 log2 fold change. To compare gene expression in drug treated samples to that in the DMSO control samples, log fold changes and pvalue were calculated for each gene, which were further used as the inputs for GSEA analysis with the R package ClusterProfiler.[53]

Data integration and label transfer

To compare cells in our data with other human brain datasets, an adult human brain single-cell dataset (GSE118257) was downloaded from the GEO and only cells from healthy donors were included. Standard preprocessing was done on the reference data. The anchors between the reference data and our data were found by using the FindTransferAnchors function in Seurat[60] using the default parameters. The cells in our data were classified based on the reference data using the TransferData function, and a prediction ID and a prediction score were assigned to each cell in our data. pHeatmap package in R was used to generate the prediction score heatmap.

Gene set enrichment analysis

To conduct gene set enrichment analysis, genes were ranked by the product of the sign of log2(fold change) and - log10(p-value). Ranked gene lists were used as input for gseGO function in package ClusterProfiler with minGSSize = 15, maxGSSize =500, nPerm = 10,000, and pvalue cutoff = 0.05.

Pseudotime trajectory analysis

Pseudotime trajectory analysis was performed using Monocle 3.[61] Firstly, the count matrix, cell metadata, as well as dimensional reduction result stored in the Seurat object was used to create a new cds object. The trajectory graph was learned by utilizing the learn_graph function with default settings. The order_cells function was used to calculate pseudotime by setting the node in the mitotic cell cluster CyP1 as the root node of the trajectory. Differentially expressed genes along the trajectory from the CyP1 to the oligodendrocytes were identified by using a generalized linear model against the pseudotime.

QUANTIFICATION AND STATISTICAL ANALYSIS

All qRT-PCR data are presented as a fold change in RNA normalized to the expression of two housekeeping genes: either *GAPDH* and *ACTB* or *GAPDH* and *CREBBP*. qRT-PCR data was analyzed using CFX Maestro

(Biorad) qPCR analysis software and graphed using Prism (GraphPad, V9). Statistical differences in qTR-PCR were determined by two-way ANOVA. Statistical differences in flow cytometric analysis were compared by a two-tailed t test. For high-throughput screening any compounds that showed increase in secNLuc activity that were greater than two standard deviations above the DMSO vehicle control were considered initial hit. Quantification of percent MBP+ cells in human OPCs upon treatment with the molecules was performed using imageJ, cell count.[52] For the primary mouse OPCs, the cells were imaged on the Opera Phenix (Perkin Elmer), 21 images per well were analyzed and quantification performed using the built-in Harmony software 4.9 (Perkin Elmer).